applied sciences

MDPI

Article

Burst-Aware Cascade Detection of UAV Radio-Frequency Signals Using Energy and Cyclostationary Analysis

Ivan Sova [1], Oleksiy Kozlov [1], Yuriy Kondratenko [1], Igor Atamanyuk [2,3,*] and Anna Aleksieieva [4]

[1] Department of Intelligent Information Systems, Petro Mohyla Black Sea National University, 54003 Mykolaiv, Ukraine; owlvano@gmail.com (I.S.); kozlov_ov@ukr.net (O.K.); y_kondrat2002@yahoo.com (Y.K.)
[2] Department of Applied Mathematics, Warsaw University of Life Sciences, 02787 Warsaw, Poland
[3] Department of Higher and Applied Mathematics, Mykolaiv National Agrarian University, 54020 Mykolaiv, Ukraine
[4] Department of Ecology, Petro Mohyla Black Sea National University, 54003 Mykolaiv, Ukraine; anna.aleksyeyeva@chmnu.edu.ua
* Correspondence: ihor_atamaniuk@sggw.edu.pl

Abstract

The increasing activity of unmanned aerial vehicles (UAVs) has intensified the demand for reliable and computationally efficient methods for passive radio-frequency (RF) signal detection. In practical RF monitoring scenarios, the environment is often non-stationary and affected by varying noise conditions. Under such circumstances, classical energy-based detectors are sensitive to noise uncertainty, while more robust approaches, such as cyclostationary analysis, require substantially higher computational resources. This work presents a burst-aware cascade method for UAV RF signal presence detection that explicitly addresses this trade-off. The proposed framework combines fast energy-based screening with temporal burst aggregation, applying spectral correlation function (SCF) analysis selectively and only when sustained signal activity is indicated. Detection is performed on fixed-length RF signal chunks, while additional segment-level duration constraints are used to characterize sustained transmissions. The method is evaluated using the publicly available DroneRF dataset and compared against six baseline detectors, including fixed-threshold energy, wavelet-based, blind cyclostationary, two adaptive energy detector variants, and a lightweight convolutional neural network. Experimental results confirm that chunk-level detection remains difficult for all considered methods. Temporal aggregation across longer intervals yields a substantial improvement: the cascade achieves $P_d = 1.000$ and AUC = 1.000 at the segment level, matching exhaustive cyclostationary detection while reducing per-segment processing time by a factor of 2.46. An additional result is that burst-level concatenation prior to SCF estimation provides implicit coherent integration, preserving $P_d = 1.000$ at signal amplitude reductions of up to -20 dB where standalone detectors degrade to $P_d = 0.995$. Overall, burst-aware cascade architectures offer a practical and interpretable approach to RF-based UAV monitoring, providing a well-grounded compromise between detection reliability and computational efficiency under realistic operating conditions.

Keywords: UAV detection; RF signal presence detection; cascade detection; cyclostationary analysis; energy detection; burst-based detection; spectrum monitoring; passive sensing

Check for updates

Academic Editors: Hicham Klaina and Peio Lopez-Iturri

Received: 19 April 2026
Revised: 24 May 2026
Accepted: 29 May 2026
Published: 3 June 2026

Copyright: © 2026 by the authors. Licensee MDPI, Basel, Switzerland. This article is an open access article distributed under the terms and conditions of the Creative Commons Attribution (CC BY) license.

1. Introduction

Unmanned aerial vehicles (UAVs) have become widely adopted across a broad range of civilian and industrial applications, including monitoring, inspection, logistics, and intelligent control systems. Their rapid proliferation has introduced new challenges related to airspace safety, regulatory compliance, and security [1–3].

The widespread adoption of these platforms in civilian, industrial, and security-related domains has led to a growing demand for reliable monitoring and detection technologies. UAV platforms support numerous beneficial applications, including aerial imaging, infrastructure inspection, and logistics. At the same time, their increasing availability introduces concrete security risks: unauthorized UAV incursions near airports have caused significant flight disruptions and economic losses, while uncontrolled drone activity poses persistent threats to critical infrastructure and public safety [4]. Privacy violations through unregulated aerial surveillance represent a further concern in densely populated environments [5,6]. As a result, the problem of UAV detection has become an active research topic across several scientific and engineering fields. Recent survey studies further emphasize the growing relevance of passive and non-cooperative sensing approaches for UAV detection, particularly in complex urban environments where traditional radar- and vision-based systems are limited [7,8].

Among existing detection modalities, passive radio-frequency (RF) sensing is often regarded as a particularly practical solution. In contrast to vision- or radar-based systems, RF-based methods do not require line-of-sight conditions and remain operational under adverse weather, low visibility, or dense urban environments [9,10]. In addition, RF monitoring enables long-range detection without relying on any form of cooperation from the UAV, which is essential for identifying both authorized and unauthorized platforms. These properties make RF-based techniques well-suited for continuous spectrum monitoring and early-warning tasks [11]. In addition, RF-based UAV detection has been shown to be effective for identifying micro- and small UAV platforms based on their communication emissions and device-specific RF characteristics, even in non-line-of-sight scenarios [12].

Despite these advantages, reliable RF-based UAV signal detection remains challenging in practice. Real-world RF environments are highly non-stationary and frequently dominated by noise and interference from diverse wireless systems. UAV transmissions are typically intermittent and bursty, may span multiple frequency bands such as 2.4 GHz and 5.8 GHz, and are often weak or partially overlapped with other signals. These effects are further amplified by air-to-ground propagation characteristics at low altitudes, where shadowing, building density, and elevation-dependent path loss introduce additional variability into the received RF signals [13]. Together, these factors make it difficult to distinguish UAV-related RF activity from background emissions in realistic monitoring scenarios.

A wide range of signal presence detection methods has been proposed to address these challenges. Classical energy-based detectors are commonly used due to their simplicity and low computational requirements; however, their performance degrades significantly under noise uncertainty and varying interference conditions. From a theoretical perspective, it has been shown that reliable signal detection at low signal-to-noise ratios is fundamentally limited under noise uncertainty, regardless of detector design or threshold optimization [14,15]. Recent work has further explored the data-driven estimation of noise levels directly from spectrum sensing signals as a means of reducing sensitivity to noise uncertainty in practical monitoring scenarios [16]. More advanced techniques, including cyclostationary and time–frequency-based methods, exploit structural signal properties and offer improved robustness, but at the expense of higher computational cost. In parallel, learning-based approaches operating on time–frequency representations have shown promising detection accuracy, although they typically require large training datasets, introduce additional la-

tency, and provide limited interpretability [17,18]. Recent learning-based spectrum sensing studies further demonstrate that high detection accuracy often comes at the cost of increased computational complexity, training data requirements, and reduced interpretability, which can limit their applicability in continuous spectrum monitoring scenarios [19].

Consequently, many existing approaches exhibit a fundamental trade-off between detection reliability and computational efficiency. Lightweight methods often fail under realistic RF conditions, while more sophisticated techniques are difficult to deploy for continuous, large-scale spectrum monitoring. Similar trade-offs between sensing reliability, temporal resolution, and computational complexity have been extensively discussed in the spectrum sensing and cognitive radio literature [20,21]. This highlights the need for RF detection methods that maintain high reliability while remaining computationally efficient and that explicitly exploit the temporal structure of UAV transmissions.

To address this need, this work proposes a burst-aware cascade RF signal detection method for UAV monitoring. The approach integrates energy-based screening, wavelet-based analysis, and cyclostationary feature extraction within a unified cascade architecture. Computationally intensive processing stages are activated only when supported by the temporal evidence of signal activity, while burst-level aggregation is used to capture the inherent temporal structure of UAV RF emissions. The resulting method aims to achieve reliable UAV signal presence detection with reduced computational complexity, making it suitable for practical RF monitoring applications.

The remainder of this paper is organized as follows. Section 2 reviews related works on RF-based signal detection, including classical energy-based methods, cyclostationary and time–frequency techniques, learning-based approaches, and cascade detection architectures. Section 3 describes the proposed burst-aware cascade detection framework, including the dataset, preprocessing steps, baseline detection methods, and the design of the cascade architecture. Section 4 presents experimental results and evaluates detection performance and computational efficiency at both chunk and segment levels. Section 5 discusses the obtained results, practical implications, limitations, and possible extensions of the proposed approach. Finally, Section 6 concludes the paper and outlines directions for future research.

2. Related Works

Research on radio-frequency-based signal detection and spectrum monitoring has produced a wide range of methods that differ in detection reliability, computational cost, and suitability for practical deployment. Existing approaches are commonly grouped into classical signal processing techniques, higher-order statistical methods, time–frequency analysis, and learning-based methods. Each class offers specific strengths, but also exhibits limitations when applied to real-world RF monitoring tasks. This section reviews the most relevant research directions and outlines how the proposed work relates to existing studies.

2.1. Energy-Based Signal Detection

Energy-based detection is among the most extensively studied techniques for RF signal presence detection due to its conceptual simplicity and minimal computational requirements [22]. In its basic form, the method compares the measured signal energy within a predefined observation window to a fixed or adaptive threshold. Because of their low processing overhead, energy detectors are widely used in real-time and wideband spectrum monitoring applications [23].

However, the performance of energy-based detectors is highly sensitive to noise uncertainty, interference, and non-stationary channel conditions. In low signal-to-noise ratio environments, or when signals exhibit bursty and intermittent behavior, energy detection often suffers from reduced reliability and increased false alarm rates [24,25]. Numer-

ous improvements, including adaptive thresholding strategies and hybrid energy-based schemes, have been proposed to address these issues [26–28]. Adaptive signal processing and neural network-based receiver architectures have also been explored in related domains, demonstrating the broader applicability of these principles beyond traditional RF environments [29,30]. Nevertheless, when used as a standalone solution, energy detection remains fundamentally limited in challenging RF environments.

2.2. Cyclostationary and Higher-Order Statistical Methods

Cyclostationary detection methods exploit periodic statistical properties that are inherent to many communication signals, such as symbol timing, modulation structure, and carrier-related periodicities [31]. By analyzing spectral correlation functions or related cyclic features, these techniques are able to distinguish structured signals from stationary noise, providing improved robustness compared to simple energy-based detectors.

This robustness makes cyclostationary analysis particularly effective in low signal-to-noise ratio conditions and in environments with strong background interference. At the same time, accurate estimation of cyclostationary features requires long observation intervals and computationally intensive processing. As a result, the direct application of these methods is often impractical for continuous, wideband, or large-scale spectrum monitoring systems [32]. These computational constraints become especially pronounced in wideband monitoring scenarios, where exhaustive cyclostationary analysis across multiple frequency bands and time windows leads to prohibitive processing overhead [33].

To mitigate these limitations, several studies have explored reduced-complexity or adaptive cyclostationary detection schemes, frequently combined with preliminary screening stages [34–36]. While such approaches reduce the overall processing burden, cyclostationary analysis remains significantly more expensive than simpler detection techniques. This has motivated its selective or conditional use within multi-stage detection methods.

2.3. Time–Frequency and Wavelet-Based Approaches

Time–frequency analysis techniques have been widely investigated as a means of improving detection sensitivity for non-stationary and transient RF signals [37]. By jointly representing signal behavior in the time and frequency domains, these methods are better suited for signals whose spectral characteristics evolve over time. Within this category, wavelet-based approaches have attracted particular interest due to their multi-resolution analysis capabilities, allowing localized examination of signal components across multiple time scales and improved sensitivity to short-duration or burst-like activity that may be poorly captured by fixed-resolution spectral methods [38–43].

These benefits, however, come at the cost of increased computational complexity. Wavelet-based detection requires careful selection of the wavelet basis, decomposition level, and associated parameters, all of which can significantly affect detection performance [44]. In addition, the effectiveness of time–frequency and wavelet-based methods depends strongly on the temporal structure of the target signals, which limits their robustness when signal characteristics are uncertain or variable. This can restrict their applicability in real-time or large-scale monitoring scenarios.

2.4. Learning-Based RF Signal Detection

In recent years, machine learning and deep learning techniques have gained increasing attention for RF signal detection and classification tasks. Unlike classical model-driven approaches, learning-based methods aim to automatically extract discriminative features from raw RF signals or from time–frequency representations such as spectrograms. Convolutional neural networks and related architectures are widely used in this context and have demonstrated high detection and classification accuracy under controlled experimental

conditions [45,46]. Recent studies have further explored deep learning architectures for spectrum sensing, including temporal convolutional networks and transfer learning strategies, reporting strong detection performance under specific training conditions [19,47]. Generative adversarial network architectures have also been explored for UAV-specific RF signal classification, demonstrating effective discrimination of illegal UAV transmissions from background wireless activity using software-defined radio platforms [48].

Learning-based RF detection methods have been applied to tasks including signal presence detection, modulation recognition, and UAV identification [18,49]. In particular, RF fingerprinting combined with deep learning techniques has been shown to enable reliable identification of UAV platforms based on their communication emissions, provided that signal-bearing segments are accurately isolated prior to feature extraction and classification [50]. However, trained models may generalize poorly to unseen signal types, interference conditions, or hardware platforms [51], and their deployment in continuous, real-time spectrum monitoring systems—especially on resource-constrained platforms—remains an open research problem [52].

Beyond classification-oriented deep learning, reinforcement learning has been explored as a means of achieving adaptive resource management in wireless sensing systems. Q-learning-based approaches have demonstrated that intelligent, state-aware decision policies can substantially improve communication efficiency under dynamic channel conditions [53]. While such methods have been applied primarily in the context of MAC protocol optimization, the underlying principle of adaptive, computationally selective processing under uncertainty is closely related to the cascade's burst-aware gating mechanism.

2.5. Cascade and Multi-Stage Detection Methods

To balance detection reliability and computational efficiency, cascade and multi-stage detection architectures have been proposed for RF signal monitoring [35]. In such methods, simple and computationally inexpensive detectors serve as initial screening stages, while more complex and robust methods are applied only to candidate signal regions. This hierarchical strategy aims to reduce unnecessary computation while preserving acceptable detection performance.

Cascade-based approaches have been widely studied in spectrum sensing and cognitive radio applications, where rapid identification of occupied or vacant frequency bands is required under strict timing constraints. Typical designs combine energy-based detection with feature-based techniques such as cyclostationary or higher-order statistical analysis to improve robustness at low signal-to-noise ratios [34,36]. Adaptive thresholding strategies have also been incorporated into multi-stage sensing pipelines as a means of reducing sensitivity to noise uncertainty, with studies demonstrating that dynamically estimated detection boundaries can improve robustness over fixed-threshold approaches under varying channel conditions [26,34,35,54]. These studies demonstrate that selectively invoking computationally expensive detectors can substantially reduce sensing time compared to exhaustive analysis.

Multi-stage architectures have more recently been applied to UAV-specific RF detection tasks. Ezuma et al. proposed a two-stage system in which a Markov model-based naïve Bayes detector first identifies the presence of RF activity, followed by an ML-based classifier that distinguishes UAV controller signals from Wi-Fi and Bluetooth interference [55]. A similar hierarchical strategy was adopted in a compressed-sensing-based approach, where a DNN-based presence detector precedes CNN classifiers responsible for UAV type and flight mode identification [56]. These works demonstrate the practical benefits of decomposing UAV RF monitoring into sequential detection and classification stages. However, they focus primarily on classification accuracy rather than computational efficiency, and do not

explicitly exploit the burst-like temporal structure of UAV transmissions as a mechanism for gating expensive processing stages.

However, many existing cascade methods rely on simplifying assumptions, such as stationary signal characteristics or predefined signal models [34,54]. Moreover, prior work has largely focused on instantaneous or window-based decisions, with limited attention given to the temporal evolution of signal activity. In particular, explicit exploitation of burst-level behavior, which is common in UAV RF transmissions, has received relatively little consideration in existing multi-stage designs. Although temporal modeling of spectrum usage has been investigated in cognitive radio research, these models are rarely integrated directly into cascade detection architectures for practical RF monitoring systems [57].

These limitations motivate the development of cascade detection methods that explicitly account for temporal signal structure while maintaining computational efficiency. Incorporating burst-level aggregation and duration-based constraints represents a promising direction for improving detection reliability in realistic, non-stationary UAV RF monitoring environments.

2.6. Research Gaps and Motivation

Overall, existing studies indicate that no single RF signal detection approach simultaneously achieves high detection reliability, low computational complexity, and robustness in interference-dominated, non-stationary RF environments. Energy-based methods offer efficient screening but are vulnerable to noise uncertainty and intermittent transmissions. More advanced techniques, such as cyclostationary and time–frequency analysis, provide improved detection capability but incur substantial computational cost, limiting their use in continuous or large-scale monitoring systems. Learning-based approaches further enhance detection performance but introduce challenges related to data availability, generalization, interpretability, and deployment complexity.

These observations highlight a persistent trade-off between detection performance and computational efficiency that remains insufficiently addressed in the context of UAV RF monitoring. In particular, relatively little attention has been paid to detection methods that explicitly exploit the burst-like temporal structure of UAV transmissions while activating computationally intensive processing only when supported by observed signal activity.

This work is motivated by the need for a lightweight yet reliable RF detection method that bridges the gap between classical signal processing methods and practical monitoring requirements. By combining burst-aware temporal aggregation with a cascade detection strategy, the proposed approach seeks to achieve robust UAV signal presence detection under non-stationary RF conditions while maintaining reduced computational complexity, making it suitable for real-time and resource-constrained monitoring applications.

The aim of this research is to design and experimentally evaluate an RF signal detection method for UAV monitoring that explicitly accounts for the bursty and intermittent nature of UAV transmissions while keeping computational complexity low. The focus is not on introducing a new detector, but on organizing well-established signal processing techniques into a cascade structure that allows expensive analysis to be applied only when there is clear temporal evidence of sustained signal activity. By combining energy-based screening, burst-level aggregation, and selective cyclostationary analysis, the proposed method targets reliable UAV signal presence detection in non-stationary RF environments without requiring exhaustive processing of all data.

The main contributions of this paper are summarized as follows:

1. A burst-aware RF signal detection method for UAV monitoring is proposed, in which signal presence is evaluated using temporally aggregated evidence rather than isolated short-time observations.

2. A cascade detection strategy is designed that combines energy-based screening, burst-level aggregation, and selective cyclostationary analysis to reduce unnecessary computational processing.
3. A duration-constrained segment-level detection mechanism is introduced to explicitly distinguish sustained UAV RF activity from short-lived interference in non-stationary spectrum conditions.
4. An experimental study is conducted on an open-source UAV RF dataset to evaluate the proposed method against six baseline detectors, spanning classical signal processing and learning-based approaches, in terms of detection performance, computational efficiency, and robustness under reduced signal amplitude.
5. An additional finding is reported: burst-level concatenation prior to SCF estimation provides implicit coherent integration, improving detection reliability at reduced signal amplitudes where standalone detectors degrade.

3. Materials and Methods

3.1. Dataset Description

This study uses the DroneRF dataset, a publicly available radio-frequency (RF) dataset designed to support research on unmanned aerial vehicle (UAV) detection and RF signal analysis [18]. The dataset was introduced to address the limited availability of open RF recordings of UAV communications and has since been widely used for benchmarking RF-based UAV detection and identification methods.

DroneRF consists of RF recordings collected under controlled experimental conditions using software-defined radio receivers. Recordings were acquired at a sampling rate of 80 MHz using two synchronized receivers capturing adjacent sub-bands: a low-band receiver covering the 2.4 GHz ISM range and a high-band receiver covering the 5.8 GHz range. Both sub-bands are used in this work. The dataset includes recordings containing UAV communication activity as well as background RF noise captured in the absence of UAV transmissions. Background recordings are intended to represent realistic ambient RF environments and are used as negative examples in signal presence detection experiments.

Three UAV platforms are represented in the dataset: Parrot Bebop, Parrot AR Drone, and DJI Phantom. UAV-related recordings are organized according to Binary Unique Identifiers (BUIs), where each BUI corresponds to a specific UAV platform and communication configuration. The background noise class corresponds to BUI 00000. The Parrot Bebop is represented by BUIs 10000, 10001, 10010, and 10011; the Parrot AR Drone by BUIs 10100, 10101, 10110, and 10111; and the DJI Phantom by BUI 11000. For each BUI, multiple recordings are provided and further divided into segments representing continuous temporal intervals containing either UAV activity or background noise. The dataset comprises 227 segments in total: 41 background noise segments and 186 signal segments distributed across the drone BUIs.

Three temporal units are used consistently throughout this work. A chunk is a contiguous block of 4000 samples—equivalent to 50 μs at the 80 MHz sampling rate—and constitutes the atomic processing unit for all detection methods. A burst is a sequence of consecutive chunks whose energy exceeds a detection threshold for at least a minimum number of chunks. A segment is one complete recording interval for a given BUI, which may span multiple files and contain multiple bursts.

In this work, the dataset is formulated as a binary signal presence detection problem. Segments containing UAV communication activity are labeled as signal-present, while background recordings without UAV transmissions are labeled as noise-only. These labels are used consistently throughout preprocessing, detection, and evaluation to ensure uniform comparison across all detection methods.

3.2. Data Preprocessing and Chunking

Raw RF recordings are preprocessed into fixed-length signal chunks that serve as the input units for all detection and evaluation procedures. Each recording is segmented into chunks of L = 4000 samples, corresponding to a duration of 50 μs at the 80 MHz sampling rate, which defines the temporal resolution of chunk-level detection.

Two preprocessing strategies are applied depending on the recording type. For background noise recordings, uniform segmentation is performed over the entire signal duration, extracting consecutive non-overlapping chunks of equal length. This approach preserves the statistical characteristics of ambient RF noise while ensuring consistent sampling.

For recordings containing UAV activity, an energy-based localization procedure is first applied to identify time intervals with elevated signal power. Short-term energy is computed using a sliding window,

$$E[n] = \sum_{k=0}^{W-1} x^2[n+k], \tag{1}$$

where $x[n]$ denotes the discrete-time RF signal and $W = 4000$ is the sliding window length, equal to one chunk duration. This formulation captures local power variations and enables the identification of transient activity.

Candidate packet regions are detected when the short-term energy exceeds an adaptive threshold,

$$E_{\text{thr}} = \max(\gamma \cdot \max(E[n]),\ E_{min}), \tag{2}$$

where $\gamma = 0.05$ is a relative scaling factor and $E_{min} = 14.77$ enforces a minimum absolute energy constraint. This strategy reduces sensitivity to noise fluctuations while avoiding spurious detections in low-energy conditions.

Detected energy peaks are grouped into contiguous regions corresponding to potential RF packets. For each region, a fixed-length chunk is extracted around its temporal center. Let n_{start} and n_{end} denote the indices of a detected region; the chunk center is computed as

$$n_c = \left\lfloor \frac{n_{\text{start}} + n_{\text{end}}}{2} \right\rfloor, \tag{3}$$

and the corresponding chunk is defined as

$$x[n_c - L/2 : n_c + L/2], \tag{4}$$

where $L = 4000$ samples. The value of E_{min} is determined empirically from the background noise recordings and reflects the minimum energy level observed in ambient RF conditions within the DroneRF dataset.

This preprocessing suppresses long silent intervals, preserves the burst-like structure of UAV transmissions, and ensures consistent chunk lengths and comparable signal-to-noise conditions across experiments.

3.3. Signal Detection Methods

Three classical signal presence detection methods are implemented as baselines. All methods operate on the same fixed-length RF signal chunks to ensure a consistent comparison.

3.3.1. Energy-Based Detection

The energy detector computes the mean-squared amplitude of each signal chunk. Let $x[n]$ denote a discrete-time RF signal chunk of length L. The energy-based detection statistic is defined as

$$E = \frac{1}{L}\sum_{n=0}^{L-1} x^2[n]. \tag{5}$$

Due to its minimal computational cost and lack of assumptions regarding signal structure, energy detection serves as a reference method. Its performance, however, is sensitive to noise uncertainty and variations in background interference.

3.3.2. Wavelet-Based Detection

The wavelet-based detector applies a multilevel discrete wavelet transform (DWT) to each signal chunk and accumulates the energy of the resulting wavelet coefficients across multiple decomposition levels. Let $c_j[k]$ denote the wavelet coefficients at scale j. The wavelet-based detection statistic is computed as

$$E_{\text{wav}} = \sum_{j=1}^{J}\sum_{k}\left|c_j[k]\right|^2, \tag{6}$$

where J is the number of decomposition levels. This method enhances sensitivity to transient and non-stationary signal components by exploiting joint time–frequency information, at the cost of increased computational complexity and parameter dependence.

3.3.3. Blind Cyclostationary Detection

The blind cyclostationary detector exploits periodic statistical properties present in many modulated RF signals without assuming prior knowledge of modulation parameters. The detector is based on the spectral correlation function (SCF), estimated using a short-time Fourier transform (STFT) framework. For a signal chunk $x[n]$, the STFT is computed using a Hann window of length $N_{FFT} = 512$ samples with a hop size of 256 samples (50% overlap), yielding $K = 14$ time frames and $F = 257$ frequency bins per chunk.

The SCF at cyclic frequency α is estimated as the time-averaged cross-product of spectral components separated by α:

$$\hat{S}\mathrm{x}^{\alpha}(\mathrm{f}) = \frac{1}{\mathrm{K}}\sum k = 0^{K-1} X_k(f)\cdot X_k^*(f+\alpha), \tag{7}$$

where $X_k(f)$ denotes the complex STFT coefficient at frame k and frequency bin f, and $*$ denotes complex conjugation. For stationary noise, the expected value of this cross-product is zero for all $\alpha \neq 0$; for cyclostationary signals, it is non-zero at one or more cyclic frequencies corresponding to the modulation structure of the signal.

A set of $N_\alpha = 32$ candidate cyclic frequencies is scanned uniformly over the available range, yielding a cyclic frequency resolution of $\Delta\alpha = \mathrm{f_s}/\mathrm{N_{FFT}} = 80\,\mathrm{MHz}/512 = 156.25\,\mathrm{kHz}$. The detection statistic is defined as the maximum mean SCF magnitude across all scanned cyclic frequencies:

$$C = \max_{\alpha}\frac{1}{F}\sum_{f=0}^{F-1}\left|\hat{S_x^{\alpha}}(f)\right|. \tag{8}$$

By exploiting periodicities in the signal statistics, cyclostationary detection offers increased robustness in low signal-to-noise ratio conditions and in the presence of interference. However, this robustness comes at the expense of significantly higher computational cost.

3.3.4. Adaptive Energy Detection

Two variants of an adaptive energy detector (AED) are evaluated as additional baselines, both building on the chunk-level energy statistic defined in Equation (5). The variants differ in how the noise floor is estimated for threshold computation.

The first variant, AED-global, estimates the noise floor from background recordings collected prior to deployment. The mean μ_{bg} and standard deviation σ_{bg} of chunk-level energy scores are computed across all background noise chunks. Each chunk is assigned a normalized detection score:

$$z_{global}[n] = \frac{E[n] - \mu_{bg}}{\sigma_{bg}}. \tag{9}$$

The second variant, AED-perseg, estimates the noise floor directly from the energy distribution within the current segment, without relying on pre-collected background data. The noise floor mean and spread are estimated as

$$\mu_{seg} = \mathrm{pct}_{25}(E[n]), \tag{10}$$

$$\sigma_{seg} = 1.4826 \cdot \mathrm{median}\Big(\Big|E[n] - \mu_{seg}\Big|\Big), \tag{11}$$

where pct_{25} denotes the 25th percentile and the factor 1.4826 makes the MAD a consistent estimator of the standard deviation under Gaussian noise. The per-segment normalized score is then computed as

$$z_{perseg}[n] = \frac{E[n] - \mu_{seg}}{\sigma_{seg}}. \tag{12}$$

For both variants, segment-level detection is performed by applying the same duration-constrained aggregation procedure used for all other methods. AED-global is equivalent in score ordering to the fixed-threshold energy detector when background statistics are stable; AED-perseg is designed to remain operational in the absence of background calibration data, at the cost of reduced discriminability when the within-segment energy distribution is unimodal.

3.3.5. Lightweight CNN Detection

A lightweight convolutional neural network (CNN) is evaluated as a learning-based baseline for chunk-level signal presence detection. The input to the network is the log-magnitude power spectral density (PSD) of each chunk. For a chunk $x[n]$ of length $L = 4000$ samples, the one-sided discrete Fourier transform yields $F = 2001$ frequency bins. The feature vector is computed as

$$\mathrm{p_f} = \log(1 + |\mathrm{X(f)}|),\ \mathrm{f} = 0, 1, \ldots, \mathrm{F} - 1, \tag{13}$$

where $X(f)$ denotes the DFT coefficient at frequency bin f. This log-magnitude representation encodes spectral shape rather than absolute power, making the input amplitude-invariant.

The network architecture consists of two one-dimensional convolutional layers, each followed by a rectified linear unit (ReLU) activation, with the first layer using 16 filters of kernel size 11 and the second using 32 filters of kernel size 7. The output of the second convolutional layer is reduced to a 32-dimensional vector via global average pooling, which is then passed through a fully connected layer of 64 units with ReLU activation and a dropout rate of 0.3, followed by a single-unit output layer with sigmoid activation. The total number of trainable parameters is approximately 6000.

The network is trained using binary cross-entropy loss with the Adam optimizer at a learning rate of 0.001, a batch size of 64, and a maximum of 20 epochs with early stopping

at a patience of five epochs on validation loss. To prevent data leakage, cross-validation is performed at the segment level: all chunks belonging to a given segment are assigned exclusively to either the training or the test fold. A stratified five-fold cross-validation procedure is applied, with out-of-fold chunk-level probabilities aggregated to produce unbiased segment-level detection scores. Segment-level decisions are made using the same duration-constrained aggregation procedure applied to all other detection methods.

3.3.6. Threshold Estimation

For energy-based detection, the decision threshold is estimated using background noise recordings only. Energy scores are computed for noise-only chunks, and the threshold is selected to satisfy a predefined probability of false alarm P_{fa}. Specifically, the threshold is selected as the empirical $(1 - P_{\text{fa}})$-quantile of the noise energy distribution. The resulting threshold is fixed for all subsequent experiments and is applied consistently across both standalone energy detection and the cascade-based detection method.

3.4. Computational Complexity

Table 1 presents the asymptotic computational complexity of each detection method per chunk of length L, where N_{FFT} denotes the FFT size used in the STFT computation and N_α denotes the number of scanned cyclic frequencies.

Table 1. Asymptotic computational complexity of the evaluated detection methods per signal chunk.

Detection Method	Complexity Per Chunk	Dominant Operation
Energy	$\mathcal{O}(L)$	Summation over L samples
Wavelet	$\mathcal{O}(L \log L)$	DWT filter bank
Cyclostationary (SCF)	$\mathcal{O}(N_\alpha \cdot K \cdot N_{FFT} log N_{FFT})$	N_α STFTs of length N_{FFT}
AED-global	$\mathcal{O}(L)$	Identical to energy detector
AED-perseg	$\mathcal{O}(L \log L)$	Percentile and MAD estimation
CNN	$\mathcal{O}(L \log L) + \mathrm{P}$	FFT $+$ $P \approx 6000$ multiply–accumulate operations
Cascade	$\mathcal{O}(L)$ per screened chunk; $\mathcal{O}(N_\alpha \cdot K_{burst} \cdot N_{FFT} \log N_{FFT})$ per retained burst	Energy screening + selective SCF

The cascade avoids per-chunk SCF computation by restricting it to retained bursts. For a burst spanning B chunks, the SCF cost is amortized across all constituent chunks, yielding an effective per-chunk cost of $\mathcal{O}(N_\alpha \cdot N_{FFT} \log N_{FFT})$. When the cyclostationary invocation rate is below 100%, the average per-chunk cost of the cascade is strictly lower than that of exhaustive cyclostationary detection. With the parameters used in this study ($N_{FFT} = 512$, $N_\alpha = 32$, $L = 4000$), the cyclostationary stage dominates all other processing costs by at least one order of magnitude.

3.5. Proposed Cascade Detection Method

To balance detection reliability and computational efficiency, a cascade-based RF signal detection method is proposed. The method operates on fixed-length RF signal chunks and applies multiple detection stages sequentially, as illustrated in Figure 1. Unlike existing cascade spectrum sensing methods, which operate on instantaneous or short-window observations, the proposed cascade explicitly exploits the burst-like temporal structure of UAV RF transmissions to gate computationally expensive processing.

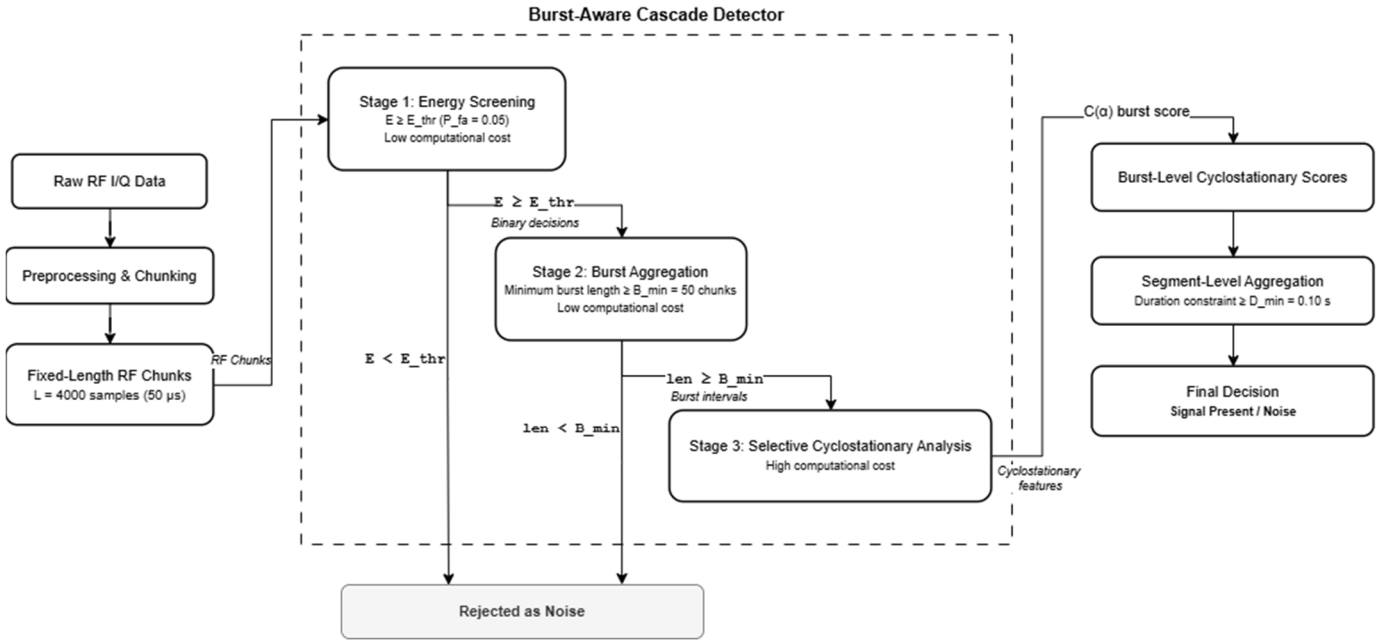

Figure 1. Diagram of the proposed cascade detection method.

The first stage applies energy-based screening to rapidly reject noise-only chunks using a threshold estimated from background data. The detection threshold is fixed at the empirical $1 - P_{fa}$ quantile of the background noise energy distribution, with $P_{fa} = 0.05$. Chunks exceeding this threshold are forwarded to subsequent stages, substantially reducing the processing load. The output of this stage is a binary sequence of chunk-level decisions $d[n] \in \{0, 1\}$, passed as input to the burst aggregation stage.

In the second stage, binary decisions from energy screening are aggregated over time to identify contiguous detection sequences, referred to as bursts. A minimum burst length constraint of $mbl = 50$ chunks is enforced to suppress isolated detections caused by impulsive noise or short-lived interference from ambient wireless sources such as Wi-Fi and Bluetooth. Bursts shorter than mbl are discarded; retained bursts are passed to the cyclostationary analysis stage as contiguous blocks of concatenated chunks.

To provide a clearer system-level view of the proposed approach, Figure 2 presents the implementation architecture of the cascade detector in a swimlane dataflow format. The low-complexity screening stage performs energy-based detection and burst construction, while the selective high-complexity stage applies cyclostationary analysis only to validated bursts. Aggregation and monitoring modules produce final segment-level decisions and performance metrics. The diagram separates the processing pipeline into a low-complexity screening stage and a selective high-complexity analysis stage, followed by aggregation and decision modules. In addition, monitoring hooks are included to collect execution time and cyclostationary invocation statistics, enabling quantitative evaluation of computational efficiency.

In the third stage, SCF-based cyclostationary analysis is applied selectively to retained bursts. By restricting computationally expensive processing to intervals exhibiting sustained activity, the cascade avoids exhaustive cyclostationary analysis while preserving robustness. The detection statistic C defined in Equation (8) is computed once per retained burst over the concatenated chunk sequence, rather than independently per chunk. This concatenation increases the number of STFT frames available for SCF estimation from $K = 14$ per individual chunk to $K \approx 4730$ per typical burst, providing implicit coherent integration.

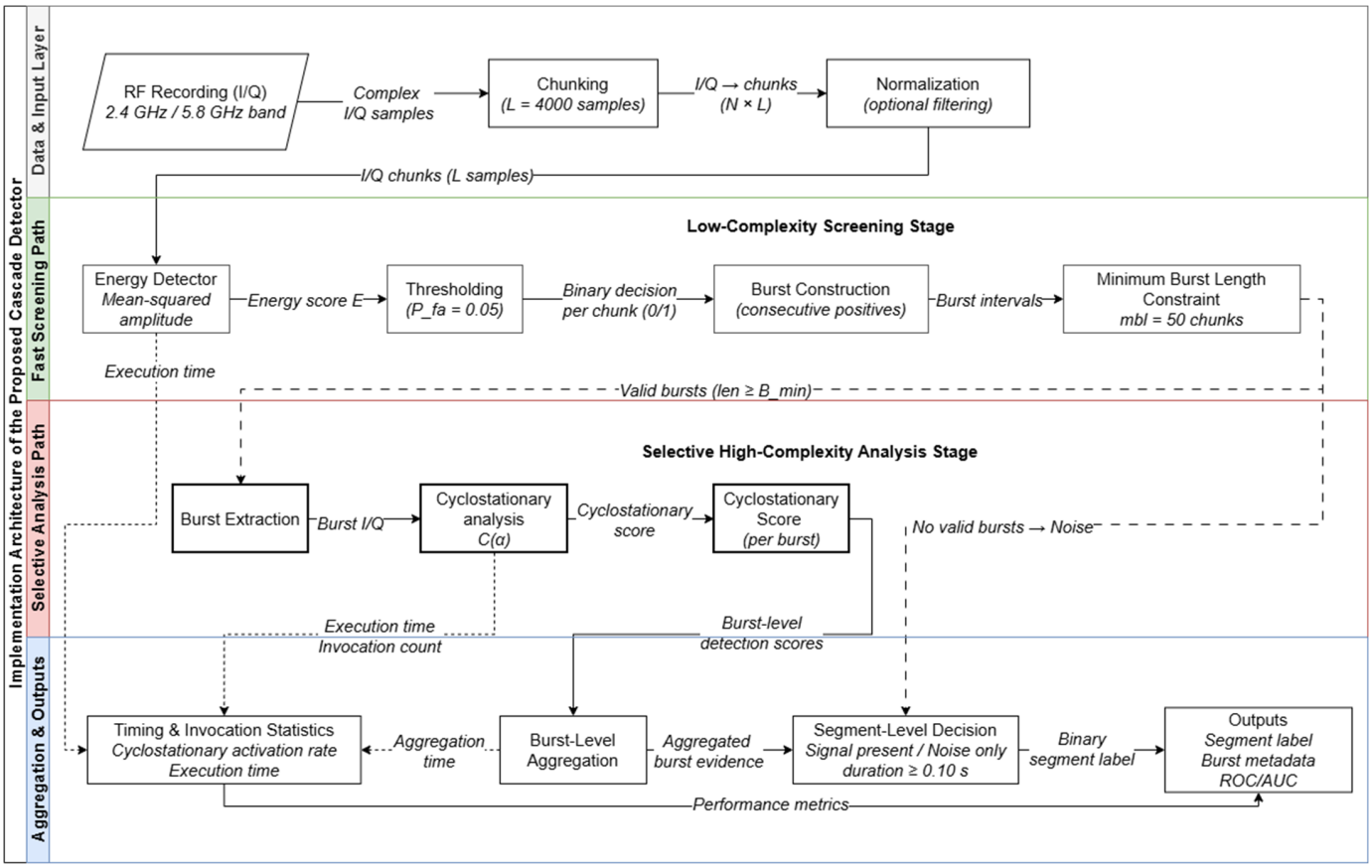

Figure 2. Implementation architecture of the proposed burst-aware cascade detector.

To further clarify the role of temporal aggregation in the proposed method, Figure 3 illustrates the relationship between chunk-level detection decisions, burst formation, and the final segment-level decision. The diagram highlights how consecutive detections form temporally coherent bursts, while isolated detections are suppressed by minimum length and duration constraints. Chunk-level energy-based decisions may be unreliable due to noise and transient interference. Consecutive detections form temporally coherent bursts, while isolated detections are discarded. Enforcing minimum burst length and duration constraints enables robust segment-level signal presence detection.

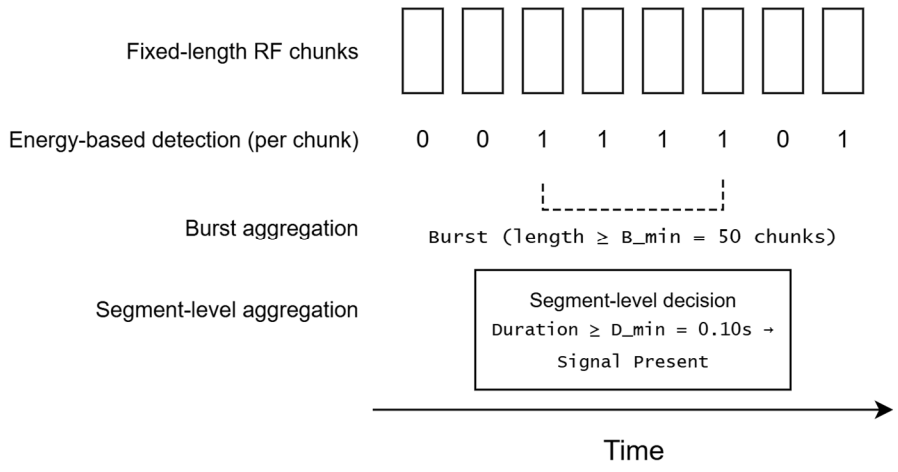

Figure 3. Illustration of temporal aggregation in the proposed burst-aware detection method.

Finally, burst-level cyclostationary outputs are aggregated to produce a segment-level detection score. A duration constraint of 0.10 s is enforced: a segment is declared signal-present only if the total duration of retained bursts exceeds this threshold. This ensures that final detections correspond to persistent RF activity rather than isolated events. Overall, the method applies advanced analysis only when supported by temporal evidence.

Algorithm 1 provides a concise formal summary of the complete cascade detection pipeline, consolidating the four processing stages described above into a single procedural specification.

Algorithm 1. Burst-Aware Cascade Detector

Input : RF recording segment $\mathcal{S}$, background noise statistics $(\mu_{bg},\ \sigma_{bg})$
Output : Segment-level binary decision $\hat{y} \in 0,\ 1$, cascade score s
Parameters : $L = 4000,\ \gamma = 0.05,\ E_{min} = 14.77,\ mbl = 50,\ d_{min} = 0.10s,$ $N_{FFT} = 512,\ N_{\alpha} = 32$

Phase 1—Energy Screening

Divide $\mathcal{S}$ into chunks x_n of length L
for each chunk x_n **do**
Compute $E[n] = \frac{1}{L}\sum_{k=0}^{L-1} x_n^2[k]$
Compute $\lambda = \max\left(\gamma \cdot \max_n(E[n]),\ E_{min}\right)$
Set d[n] $=$ 1 **if** $E[n] \geq \lambda$, **else** 0
end for

Phase 2—Burst Aggregation

Group consecutive d[n] $=$ 1 into bursts $\mathcal{B} = B_1, B_2, \ldots$
Discard any B_i where $|B_i| < mbl$
Let $\mathcal{B}^*$ denote retained bursts
if $\mathcal{B}^* = \{\ \}$ **return** $\hat{y} = 0, s = 0$

Phase 3—Selective SCF Analysis

for each retained burst B_i **do**
Concatenate chunks $\rightarrow$ burst signal b_i
Compute STFT : $X_k(f)$, Hann window, $N_{FFT} = 512$, hop = 256
for $j = 1, \ldots, N_{\alpha}$ **do**
$S^{\hat{\alpha}_j}(f) = \frac{1}{K}\sum_{k=0}^{K-1} X_k(f) \cdot X_k^*(f + \alpha_j)$
end for
$C_i = \max_{\alpha_j} \frac{1}{F}\sum_{f=0}^{F-1} \left|S^{\hat{\alpha}_j}(f)\right|$
end for

Phase 4—Segment-Level Decision

$D = \sum_i |B_i| \cdot \frac{L}{f_s}$
$s = \max_i C_i$
if $D \geq d_{min}$ **then** $\hat{y} = 1$ **else** $\hat{y} = 0$
return $\hat{y}, s$

3.6. Evaluation Metrics and Experimental Setup

Detection performance is evaluated at two temporal scales. Chunk-level evaluation considers detection scores computed independently for each fixed-length chunk, reflecting short observation windows. Segment-level evaluation aggregates chunk-level

scores over time to assess sustained RF activity, which better reflects practical UAV monitoring conditions.

Performance is assessed using ROC curves and the area under the curve (AUC) as a threshold-independent metric. In addition, the probability of detection (Pd) is evaluated at a fixed probability of false alarm (Pfa) to enable controlled comparison across methods.

Computational efficiency is measured as the average execution time per segment. For the cascade detector, execution time is decomposed into energy screening, burst aggregation, and cyclostationary analysis. The cyclostationary invocation rate—the fraction of segments triggering cyclostationary processing—is also reported to quantify cascade selectivity.

All experiments were carried out on a workstation equipped with an AMD Ryzen 7 9800X3D processor (AMD, Santa Clara, CA, USA) and 32 GB of DDR5 system memory, running Windows 11 Pro, 64-bit (Microsoft, Redmond, WA, USA). The experimental pipeline was developed in Python (v3.11, Python Software Foundation, Wilmington, DE, USA) and executed using a standard scientific computing environment.

An NVIDIA GeForce RTX 3060 graphics processing unit (NVIDIA, Santa Clara, CA, USA) was available and used during the execution of the detection and evaluation procedures. Core numerical and signal processing operations were implemented using NumPy (v2.4.0), SciPy (v1.16.3), and PyWavelets (v1.9.0), while performance metrics such as ROC curves, AUC, and detection probabilities were computed using scikit-learn (v1.8.0, INRIA, Paris, France). Figures and plots were generated using Matplotlib (v3.10.8, Matplotlib Development Team).

All baseline detectors and the proposed cascade detection framework were executed under the same hardware and software conditions. Timing measurements were obtained using high-resolution system timers and reflect the total processing time required for segment-level analysis, including all cascade stages where applicable. GPU acceleration was used exclusively for CNN inference. PSD feature extraction for the CNN baseline was performed on CPU using NumPy FFT; the resulting feature vectors were passed to the network for inference on GPU (CUDA, batch size = 256). All other detection methods—including energy-based screening, wavelet analysis, SCF-based cyclostationary detection, and all cascade stages—were executed entirely on CPU. No method benefited from hardware- or software-specific optimizations beyond those explicitly described.

The described setup corresponds to a typical contemporary research workstation and was selected to allow a consistent evaluation of both detection performance and computational cost.

4. Simulation Results

4.1. Chunk-Level Detection Performance

Chunk-level detection performance is evaluated to assess the ability of the considered signal presence detectors to operate on short RF observation windows. ROC curves are obtained for all evaluated detectors using chunk-level detection scores, as illustrated in Figure 4.

The ROC curves indicate only moderate discriminative capability for the majority of methods at the chunk level. The classical detectors—energy, wavelet, and cyclostationary—achieve nearly identical chunk-level AUC values of approximately 0.758–0.760, with no meaningful separation between them. The AED-global variant follows the energy detector exactly, as its score is a linear rescaling of the same underlying energy statistic. AED-perseg performs below the random baseline at the chunk level (AUC = 0.595), a consequence of within-segment normalization that collapses discriminability when all chunks within a segment share similar energy levels. The CNN achieves a substantially higher chunk-level

AUC of 0.951, reflecting its use of log-magnitude spectral shape features rather than raw energy; however, even at this level, chunk-level decisions remain unreliable in isolation. None of the approaches provides reliable separation between signal-present and noise-only classes when decisions are made on individual chunks.

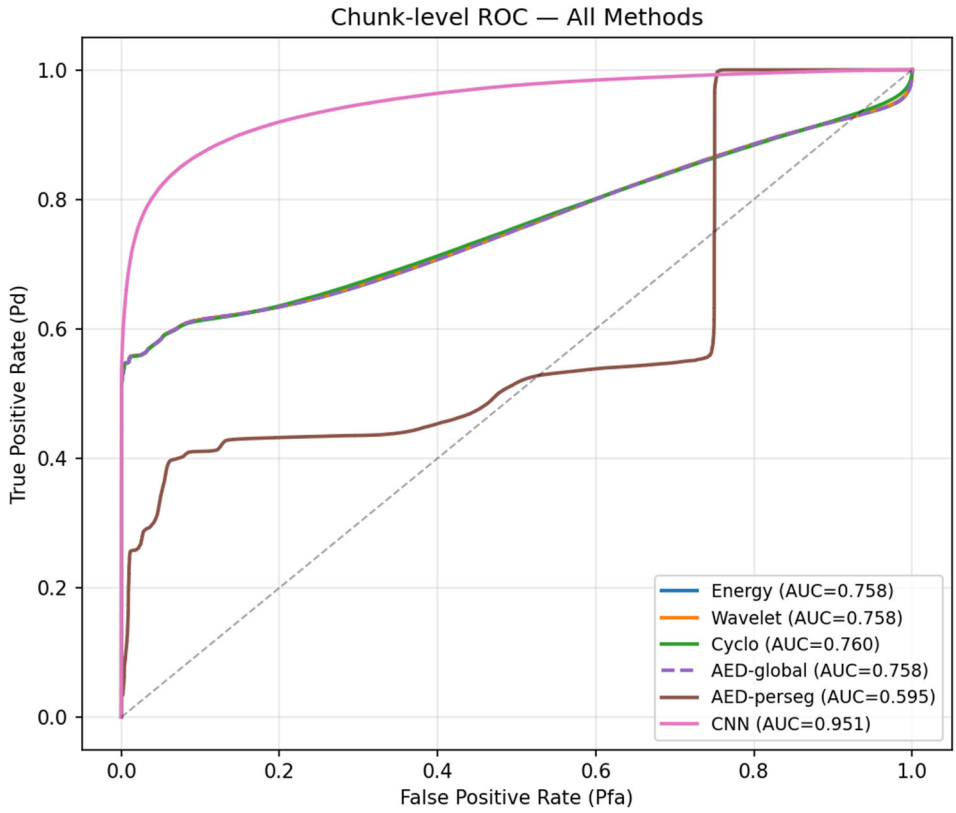

Figure 4. Chunk-level ROC curves for all energy detection methods.

This behavior highlights the intrinsic difficulty of instantaneous RF signal presence detection in non-stationary environments. Individual chunks may contain only partial signal energy, correspond to inactive portions of burst-based UAV transmissions, or be dominated by transient interference and noise. Consequently, chunk-level detection alone is insufficient for robust UAV RF monitoring and motivates the use of temporal aggregation across longer observation intervals.

4.2. Segment-Level Detection with Duration Constraint

Segment-level detection performance is evaluated by aggregating chunk-level detection scores under a duration constraint. The resulting ROC curves for all detection methods are presented in Figure 5. Compared with chunk-level evaluation, temporal aggregation leads to a substantial improvement in detection performance for all considered detectors, underscoring the importance of temporal context in the analysis of UAV RF activity.

For sustained UAV transmissions, near-perfect separation between signal-present and noise-only segments is achieved by the majority of evaluated detectors. At a target probability of false alarm of 0.05, five of the seven evaluated methods—energy, wavelet, cyclostationary, AED-global, and the cascade—reach a probability of detection of 1.000, as summarized in Table 2. The CNN achieves $P_d = 0.995$ and AUC = 0.998, marginally below ceiling owing to the cross-validation procedure used to produce unbiased out-of-fold estimates. AED-perseg is the only method that fails to achieve reliable segment-level detection, with $P_d = 0.581$ and AUC = 0.618; this outcome is expected, as within-

segment normalization collapses score discriminability when all chunks in a segment share uniformly high or uniformly low energy levels.

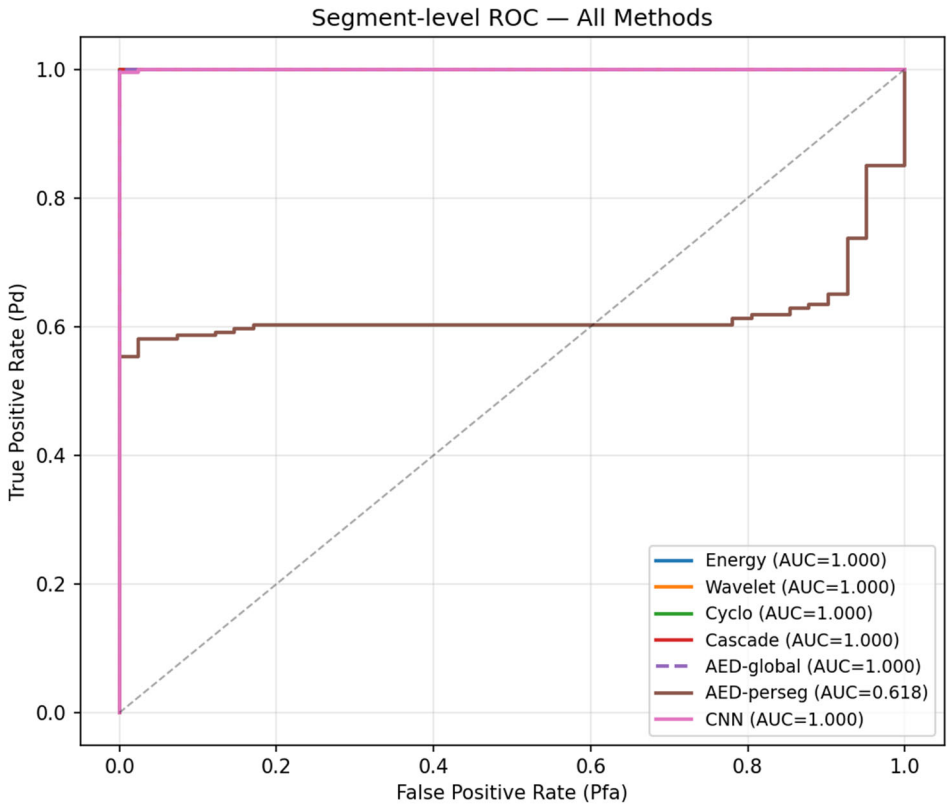

Figure 5. Duration-constrained segment-level ROC curves for all evaluated detection methods.

Table 2. Segment-Level Detection Performance at Fixed Probability of False Alarm (Pfa = 0.05).

Detection Method	Pd	Pfa	AUC
Energy	1.000	0.000	1.000
Wavelet	1.000	0.000	1.000
Cyclostationary (SCF)	1.000	0.000	1.000
AED-global	1.000	0.000	1.000
AED-perseg	0.581	0.049	0.618
CNN	0.995	0.024	0.998
Cascade	1.000	0.000	1.000

The observed perfect segment-level performance represents an upper bound achievable under controlled experimental conditions with long and continuous signal activity. It should not be interpreted as instantaneous or real-time detection capability. Instead, these results illustrate how temporal aggregation fundamentally alters the detection problem by emphasizing sustained RF activity rather than isolated short-term observations.

The proposed cascade detector achieves a segment-level AUC of 1.000 and $P_d = 1.000$ at the $P_{fa} = 0.05$ operating point, matching exhaustive cyclostationary detection while reducing per-segment processing time by a factor of 2.46, as reported in Table 3. This outcome reflects the characteristics of the evaluated dataset and the adopted segment-level aggregation strategy, rather than an inherent limitation of the detection methods themselves.

Table 3. Average execution time of each detection method per segment (mean ± standard deviation, 95% confidence interval, N = 227).

Detection Method		Mean, ms	Std, ms	95% CI, ms
Energy		19.38	15.32	±1.99
Wavelet		171.78	132.88	±17.29
Cyclostationary (SCF)		2074.57	1608.97	±209.31
AED-global		20.06	15.36	±2.00
AED-perseg		19.52	15.03	±1.96
CNN	PSD extraction (CPU)	54.97	—	—
	Inference (GPU, CUDA)	22.52	—	—
	Total	77.48	63.14	±8.21
Cascade	Energy	18.96	15.07	±1.96
	Burst aggregation	0.10	0.08	±0.01
	Cyclostationary	823.84	1001.25	±130.25
	Total	842.91	1015.48	±132.10

The observed ceiling-level performance across the majority of methods is a consequence of the DroneRF's controlled recording conditions, which feature sustained, high-SNR UAV transmissions with clearly distinct spectral characteristics. Under these conditions, temporal aggregation is sufficient to achieve near-perfect separation regardless of the detection method employed. The differentiating factors between methods—computational efficiency, robustness under reduced signal amplitude, and dependence on labeled training data—are examined in subsequent sections.

4.3. Computational Efficiency and Selectivity

Computational efficiency is evaluated by measuring the average execution time per segment for each detection method. The results are summarized in Table 3. As expected, the standalone energy-based detector exhibits the lowest execution time, whereas blind cyclostationary detection incurs the highest computational cost.

The cascade detector achieves a substantial reduction in computational cost compared to blind cyclostationary detection. Although its total execution time exceeds that of simple energy- or wavelet-based detection, it remains significantly lower than exhaustive cyclostationary processing. The breakdown of execution time across cascade stages shows that most of the computational burden is associated with the cyclostationary stage, while energy screening and burst aggregation introduce negligible overhead.

The selectivity of the cascade detector is further examined through cyclostationary invocation statistics. Following the correction of the cyclostationary detector implementation and the adjustment of the minimum burst length constraint to $mbl = 50$ chunks, the cascade exhibits meaningful selectivity across the evaluated dataset. Across the 227 evaluated segments, cyclostationary analysis is triggered for all 186 signal-present segments (invocation rate = 100%) and for only one of the 41 background noise segments (invocation rate = 2.4%), yielding an overall invocation rate of 82.4%. This result confirms that the cascade effectively gates expensive SCF processing: noise-only segments are rejected at the energy screening stage in the vast majority of cases, while signal-present segments consistently proceed to cyclostationary analysis.

The invocation rate breakdown by class is illustrated in Figure 6. On average, 17.62 bursts are detected per signal segment, with a mean burst length of 268.97 chunks.

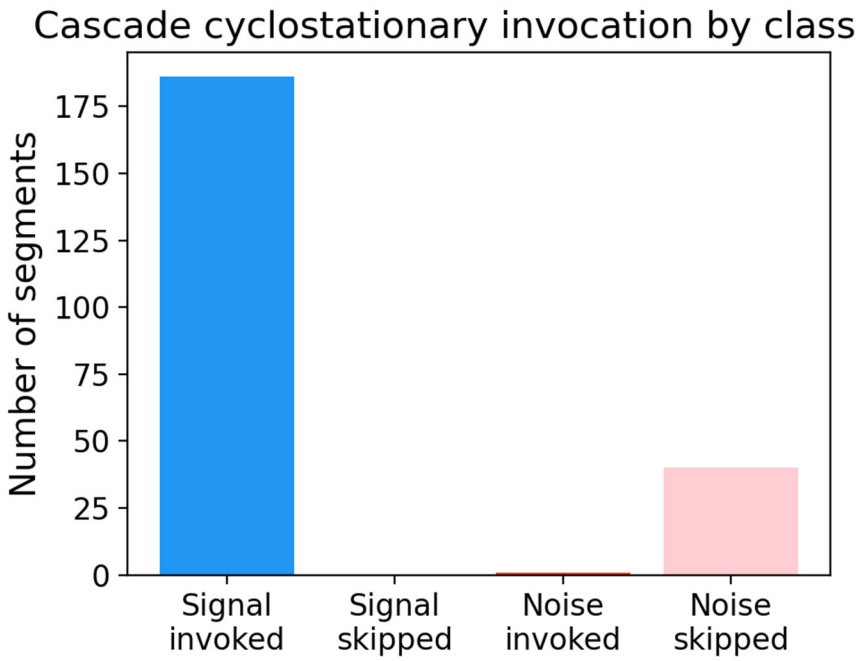

Figure 6. Cyclostationary invocation rate by segment class.

The distribution of detected burst lengths is shown in Figure 7. The substantially longer burst lengths compared to individual chunks ($B \approx 269$ vs. $K = 14$ STFT frames per chunk) confirm that burst-level concatenation provides a meaningful coherent integration gain prior to SCF estimation.

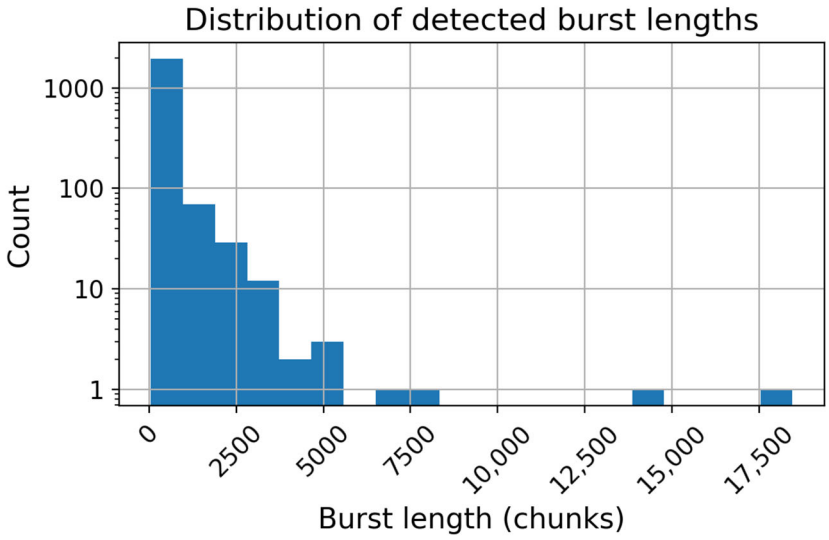

Figure 7. Distribution of detected burst lengths across signal segments, shown on a logarithmic y-axis scale to reveal the heavy-tailed structure of the distribution.

These results demonstrate that the cascade selectively applies SCF analysis based on temporal evidence of signal activity, reserving computationally expensive processing for intervals where sustained RF activity has been detected. The high standard deviation of the cascade total execution time (1015.48 ms relative to a mean of 842.91 ms) reflects the variable number of bursts retained per segment: segments with sustained signal activity incur proportionally higher cyclostationary processing time, while noise-only segments—for which cyclostationary analysis is triggered in only 2.4% of cases—complete near-instantaneously at the energy screening stage.

4.4. Parameter Sensitivity Analysis

The cascade detector exposes four key parameters: the energy screening scaling factor γ, the minimum burst length *mbl*, the SCF FFT size N_{FFT}, and the segment-level duration constraint. To assess the robustness of the proposed method to parameter choices, each parameter is varied independently while holding the remaining parameters fixed at their nominal values. Detection performance (P_d, AUC) and cyclostationary invocation rate are recorded for each configuration.

The effect of the energy screening threshold γ is illustrated in Figure 8. Detection performance remains at ceiling across all tested values. Selectivity, however, varies meaningfully: increasing γ raises the energy screening threshold, suppressing more chunks at the first stage and progressively increasing the noise-segment invocation rate. The nominal value $\gamma = 0.05$ was selected as the operating point that maintains full signal detection while keeping noise invocations near zero.

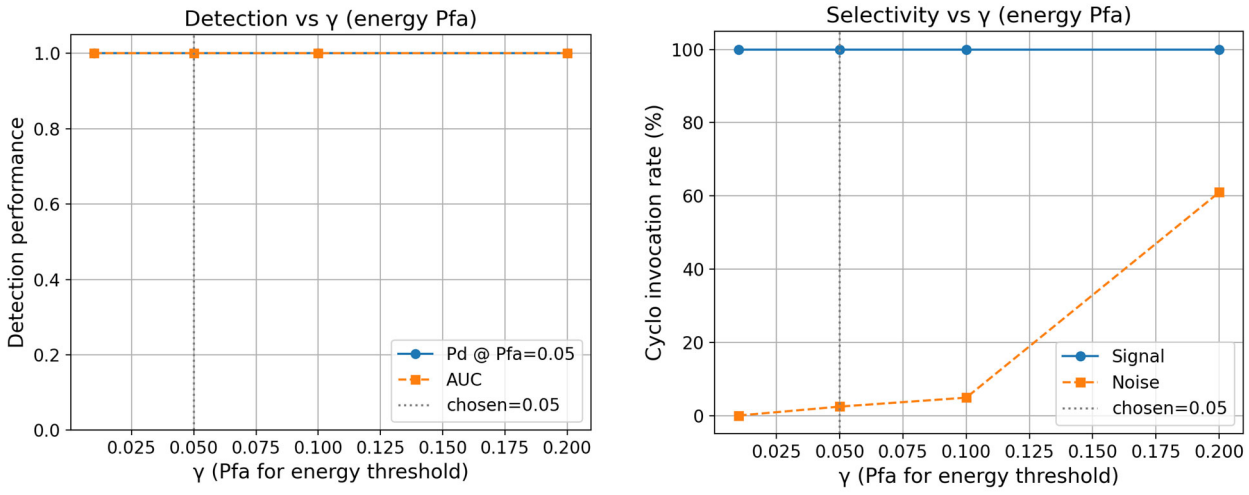

(**a**) (**b**)

Figure 8. Sensitivity of the cascade detector to the energy screening threshold γ: (**a**) detection performance (P_d at $P_{fa} = 0.05$ and AUC) as a function of γ; (**b**) cyclostationary invocation rate by segment class as a function of γ. The chosen value $\gamma = 0.05$ is indicated by a dotted vertical line.

The effect of the minimum burst length *mbl* is illustrated in Figure 9. Detection performance again remains stable at $P_d = 1.000$ across all tested values. The noise-segment invocation rate, however, drops sharply as *mbl* increases: requiring longer contiguous detection sequences filters out short-lived ambient interference bursts in background noise segments. The nominal value $mbl = 50$ chunks was selected as the point at which noise invocation drops to 2.4% while signal detection is preserved.

The effect of the SCF window size N_{FFT} is illustrated in Figure 10. Neither detection performance nor invocation rate shows meaningful variation across the tested range, confirming that N_{FFT} can be set based on computational budget without affecting detection reliability. The nominal value $N_{FFT} = 512$ provides a balance between frequency resolution and processing cost.

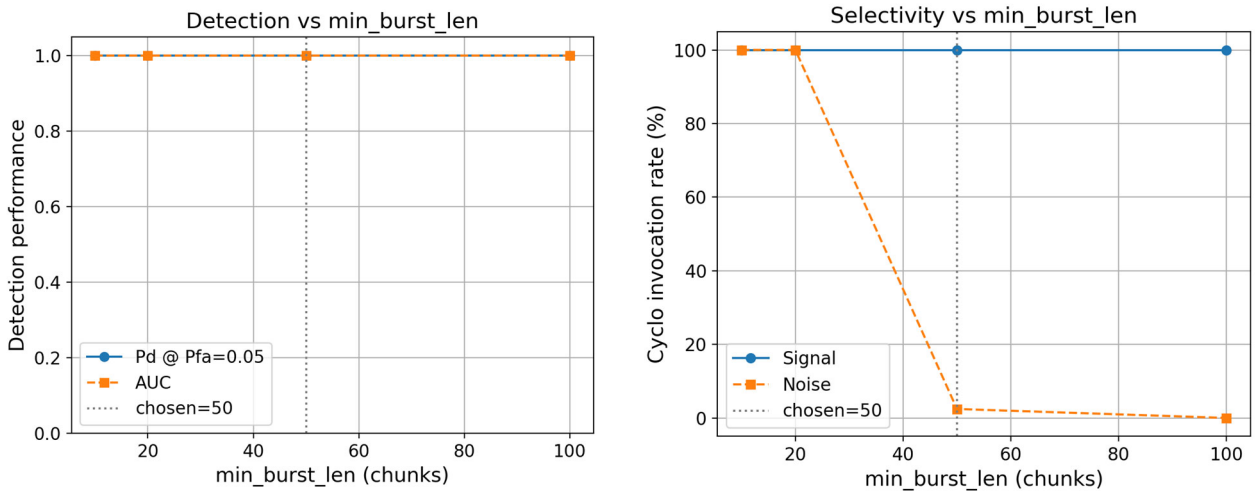

(**a**) (**b**)

Figure 9. Sensitivity of the cascade detector to the minimum burst length *mbl*: (**a**) detection performance (P_d at $P_{fa} = 0.05$ and AUC) as a function of *mbl*; (**b**) cyclostationary invocation rate by segment class as a function of *mbl*. The chosen value *mbl* = 50 chunks is indicated by a dotted vertical line.

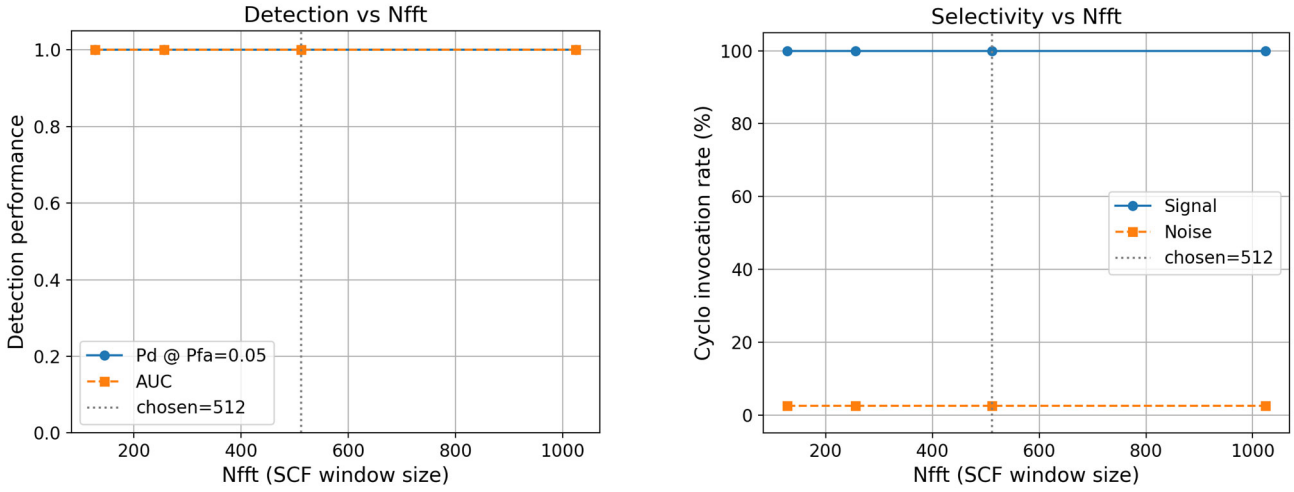

(**a**) (**b**)

Figure 10. Sensitivity of the cascade detector to the SCF window size $N_{\{FFT\}}$: (**a**) detection performance (P_d at $P_{fa} = 0.05$ and AUC) as a function of $N_{\{FFT\}}$; (**b**) cyclostationary invocation rate by segment class as a function of $N_{\{FFT\}}$. The chosen value $N_{\{FFT\}} = 512$ is indicated by a dotted vertical line.

The effect of the segment-level duration constraint is illustrated in Figure 11. Detection performance remains flat across all tested values, indicating that any threshold within the tested range is sufficient to separate sustained UAV transmissions from noise under the evaluated conditions. The nominal value of 0.10 s was selected to correspond to a minimum of two burst lengths at the chosen *mbl*.

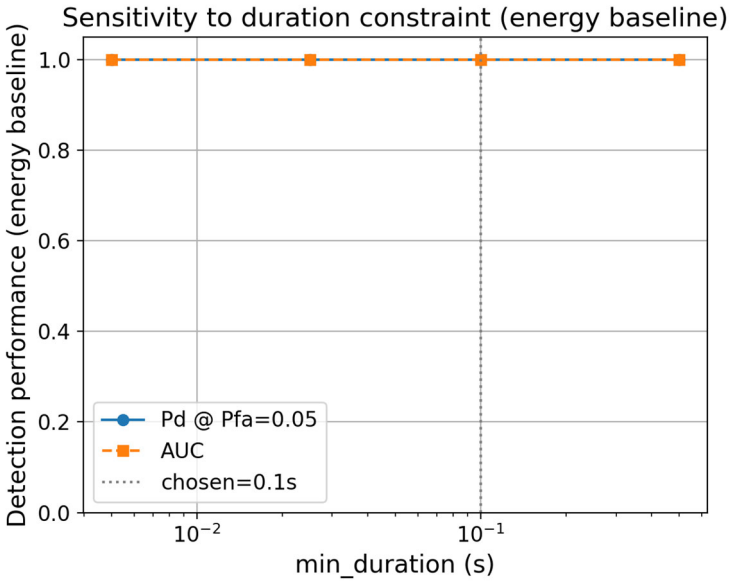

Figure 11. Sensitivity of the cascade detector to the segment-level duration constraint: detection performance (P_d at $P_{fa} = 0.05$ and AUC) as a function of the minimum duration threshold. The chosen value of 0.10 s is indicated by a dotted vertical line.

4.5. Robustness Evaluation

To evaluate detection performance beyond the nominal DroneRF conditions, two stress tests are conducted: a signal amplitude scaling experiment and a transmission duty cycle experiment. Results for all seven methods are presented in Figure 12.

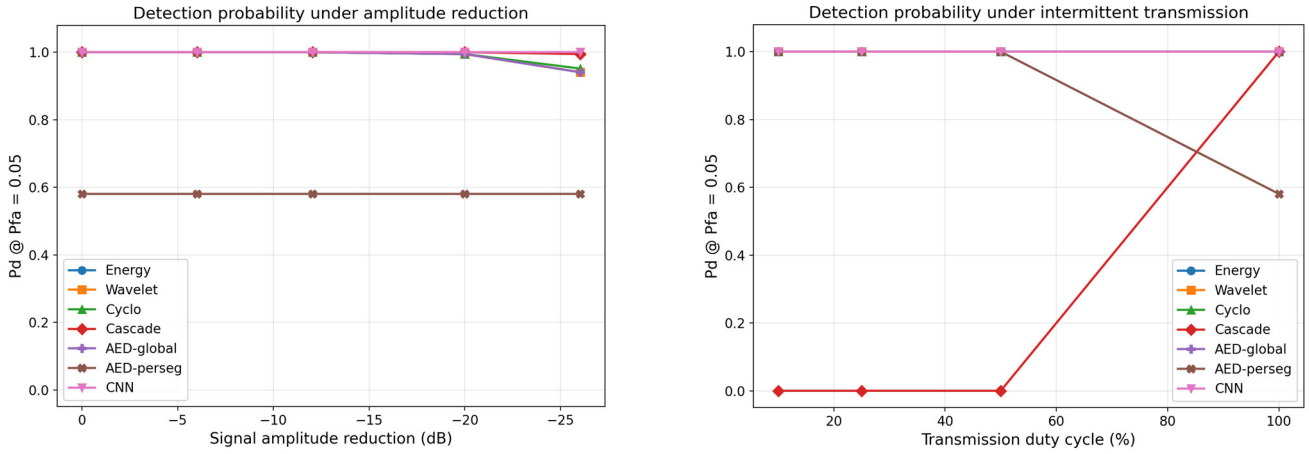

Figure 12. Robustness evaluation of all evaluated detection methods: (**a**) detection probability P_d at $P_{fa} = 0.05$ as a function of signal amplitude reduction; (**b**) detection probability P_d at $P_{fa} = 0.05$ as a function of transmission duty cycle.

Signal amplitude scaling. Signal chunk amplitudes are scaled by a factor $\alpha \in \{1.0, 0.5, 0.2, 0.1, 0.05\}$, corresponding to effective amplitude reductions of 0, −6, −14, −20, and −26 dB relative to the original recordings. All other parameters remain unchanged. Energy, wavelet, cyclostationary, and AED-global detectors maintain $P_d = 1.000$ down to −20 dB, degrading to $P_d = 0.941$ at −26 dB. The cascade maintains $P_d = 1.000$ at −20 dB and degrades more gradually to $P_d = 0.995$ at −26 dB, outperforming the standalone detectors at that operating point. This advantage arises from burst-level concatenation prior to SCF estimation: rather than processing individual 4000-sample chunks with $K = 14$

STFT frames, the cascade computes the SCF over concatenated bursts of approximately 4730 frames, providing implicit coherent integration that improves estimation quality at reduced signal amplitude. The CNN achieves $P_d = 1.000$ at all tested amplitude levels, including -26 dB. This robustness stems from the log-magnitude PSD input representation, which encodes spectral shape rather than absolute power and is therefore invariant to amplitude scaling. AED-perseg remains flat at $P_d = 0.581$ across all amplitude levels, as within-segment normalization is unaffected by uniform amplitude scaling.

Transmission duty cycle. Signal chunks are randomly zeroed with probability $1 - d$, where $d \in \{0.10, 0.25, 0.50, 1.00\}$ denotes the transmission duty cycle. Energy, wavelet, cyclostationary, AED-global, and CNN detectors maintain $P_d = 1.000$ across all tested duty cycles, as these methods operate at the individual chunk level and the duration-constrained aggregation selects the top-scoring chunks regardless of transmission gaps. The cascade collapses to $P_d = 0.000$ at duty cycles below 100%: when active chunks are interspersed with silent intervals, no contiguous sequence of length $mbl = 50$ forms and no bursts are retained. AED-perseg exhibits the inverse behavior, recovering from $P_d = 0.581$ at 100% duty cycle to $P_d = 1.000$ at duty cycles of 50% and below. At reduced duty cycles, zeroed chunks introduce a bimodal within-segment energy distribution that allows AED-perseg to reliably estimate a noise floor and recover discriminability. These two methods are thus structurally complementary: the cascade is suited for sustained continuous transmissions, while AED-perseg is better matched to intermittent protocols.

The duty cycle result defines the operating scope of the proposed cascade: it is designed for the sustained-transmission regime characteristic of UAV radio-control links, where continuous DSSS or OFDM waveforms produce uninterrupted burst activity. For detection tasks involving intermittent or low-duty-cycle signals, per-chunk detectors or within-segment adaptive methods are more appropriate.

5. Discussion

The obtained results can be understood by considering both the temporal characteristics of UAV radio-frequency transmissions and the assumptions underlying classical signal detection methods. At the chunk level, detection performance remains limited for all evaluated detectors because short RF observation windows often capture incomplete signal content. Individual chunks may correspond to inactive portions of burst-based transmissions or be dominated by transient interference and noise. Under these conditions, neither simple energy-based metrics nor more advanced feature extraction methods can reliably separate signal-present and noise-only observations. Similar behavior has been reported in prior work on spectrum sensing, where instantaneous or short-term detection is known to be unreliable in non-stationary RF environments.

Introducing temporal aggregation changes the detection problem in a fundamental way. UAV RF transmissions typically persist over time and exhibit a burst-like structure, whereas background noise and interference tend to be short-lived and weakly correlated. Aggregating detection evidence across consecutive chunks and enforcing a duration constraint shifts the task from instantaneous discrimination to identifying sustained RF activity. This explains the near-perfect segment-level separability observed for the standalone detectors in the evaluated dataset and demonstrates the critical role of temporal information in reliable UAV RF monitoring.

The proposed cascade detection method builds directly on this observation while accounting for the computational cost of advanced signal analysis. Exhaustive cyclostationary detection provides strong robustness to noise uncertainty and interference but becomes prohibitively expensive when applied uniformly. Energy-based detection, in contrast, is computationally lightweight but insufficiently reliable when used alone. The

cascade method occupies an intermediate position by combining low-cost screening and burst-level aggregation to determine when cyclostationary analysis is warranted.

Relative to fixed-threshold energy detection, the proposed cascade improves robustness by incorporating temporal consistency and selectively applying higher-order feature analysis. The AED-global variant, which applies background-calibrated z-score normalization to the energy statistic, produces identical segment-level ROC performance to the fixed-threshold energy detector—a consequence of the linear score rescaling that preserves rank ordering. This confirms that the cascade's energy screening stage is already equivalent to the strongest adaptive thresholding variant for sustained-transmission UAV signals, without requiring explicit noise floor estimation. Compared to full cyclostationary processing, the cascade reduces unnecessary computation by restricting SCF analysis to temporally coherent signal regions, achieving a 2.46× reduction in per-segment processing time while maintaining equivalent detection performance. When contrasted with the lightweight CNN baseline, the cascade is slower per segment but requires no labeled training data and invokes its expensive processing stage on only 2.4% of background noise segments. The CNN achieves higher amplitude robustness at −26 dB ($P_d = 1.000$ vs. $P_d = 0.995$) owing to its amplitude-invariant log-magnitude PSD representation; however, this advantage comes at the cost of supervised training and uniform per-chunk processing regardless of signal activity.

An unreported advantage of the cascade architecture emerges from the amplitude scaling experiment. At a signal amplitude reduction of −20 dB, standalone energy, wavelet, and cyclostationary detectors degrade to $P_d = 0.995$, while the cascade maintains $P_d = 1.000$. This improvement arises from burst-level concatenation prior to SCF estimation: by processing all chunks within a retained burst as a single concatenated signal, the cascade forms an observation of approximately 1.2 million samples, yielding $K \approx 4730$ STFT frames for SCF estimation rather than the $K = 14$ frames available per individual chunk. The resulting implicit coherent integration substantially improves SCF estimation quality at reduced signal amplitude, providing an SNR advantage that is not present in any of the evaluated standalone detectors.

A structural complementarity emerges between the cascade and AED-perseg that has practical implications for system design. The cascade achieves $P_d = 1.000$ under sustained-transmission conditions but collapses completely at duty cycles below 100%, while AED-perseg fails under sustained conditions ($P_d = 0.581$) but recovers to $P_d = 1.000$ at reduced duty cycles. This inverse behavior reflects fundamentally different operating assumptions: the cascade requires consecutive chunk activity to form bursts, while AED-perseg requires within-segment energy heterogeneity to estimate a valid noise floor. In a practical deployment where both sustained and intermittent UAV protocols may be encountered, these two detectors could be operated in parallel as complementary front-ends, with the cascade handling continuous RC link transmissions and AED-perseg covering intermittent or low-duty-cycle signals.

From a practical standpoint, the results suggest that burst-aware cascade detection is well-suited for continuous spectrum monitoring scenarios, where long observation durations and limited computational resources are common. The method can serve as a front-end detection module that flags candidate signal activity for subsequent analysis or downstream classification, enabling scalable deployment on embedded or resource-constrained platforms. Such a front-end detection stage is particularly relevant for RF fingerprinting and UAV identification pipelines, where reliable isolation of signal-bearing segments is a prerequisite for feature extraction and deep learning-based classification. The evaluated dataset, consisting of sustained high-SNR UAV transmissions recorded under controlled conditions, results in cyclostationary activation for all signal segments.

In more heterogeneous environments—where background noise dominates the majority of monitored intervals—the cascade's energy gate is expected to suppress a substantially larger fraction of incoming data, further reducing the effective computational load. From a system-design perspective, the proposed cascade framework exposes several tunable parameters, such as energy thresholds, burst duration constraints, and cascade activation policies. Systematic tuning of these parameters, as demonstrated in Section 4.4, confirms that detection performance remains stable across a wide range of values, reducing the practical burden of deployment-specific calibration.

Several limitations of the present study should be acknowledged. First, evaluation relies solely on the DroneRF dataset, which contains sustained, high-SNR UAV transmissions recorded under controlled laboratory conditions; performance under real-world multipath fading, co-channel interference, or path loss variability is not characterized. Second, the amplitude scaling and duty cycle stress tests are applied post-chunking, meaning that the effect of noise and signal degradation on the upstream energy-based preprocessing stage is not captured. Third, the cascade's burst aggregation mechanism makes it unsuitable for UAV protocols with low transmission duty cycles; in such scenarios, per-chunk or within-segment adaptive detectors are preferable. Fourth, the current evaluation is conducted offline; real-time deployment would require additional engineering effort to implement streaming preprocessing and to verify latency bounds under continuous operation.

Overall, the discussion indicates that the observed performance gains arise primarily from exploiting temporal structure and selective processing rather than increasing detector complexity. This interpretation is consistent with established findings in RF spectrum sensing and supports the proposed method as a practical system-level solution tailored to UAV RF monitoring.

6. Conclusions

This paper introduced a burst-aware cascade radio-frequency signal detection method for UAV monitoring, designed to balance detection reliability with computational efficiency. By combining energy-based screening, temporal burst aggregation, and selective cyclostationary analysis, the proposed method explicitly exploits the inherent temporal structure of UAV RF transmissions rather than relying on increasingly complex standalone detectors. The method is evaluated against six baselines spanning classical signal processing and learning-based approaches: fixed-threshold energy, wavelet-based, blind cyclostationary, two adaptive energy detector variants, and a lightweight convolutional neural network.

The experimental results demonstrate that enforcing temporal aggregation through a duration constraint is essential for reliable RF-based UAV signal detection in non-stationary spectrum environments. Sustained UAV transmissions become clearly separable from background noise at the segment level, even when relatively simple detection mechanisms are employed at the chunk level. At the segment level, five of the seven evaluated methods achieve $P_d = 1.000$ and AUC = 1.000, confirming that temporal aggregation is the dominant factor in detection performance under the evaluated conditions.

At the same time, the cascade structure limits computational overhead by selectively invoking cyclostationary analysis only for time intervals that exhibit consistent evidence of signal activity, achieving a 2.46× reduction in per-segment processing time relative to exhaustive cyclostationary detection. Cyclostationary analysis is triggered for 100% of signal-present segments and only 2.4% of background noise segments, confirming that the energy screening and burst aggregation stages together constitute an effective pre-filter. This selective processing avoids exhaustive analysis of all data while preserving high detection reliability, highlighting that uniform application of computationally expensive techniques is not a prerequisite for effective RF monitoring.

An additional finding is that burst-level concatenation prior to SCF estimation provides implicit coherent integration, maintaining $P_d = 1.000$ at signal amplitude reductions of up to -20 dB where standalone detectors degrade to $P_d = 0.995$. A structural complementarity is also identified between the cascade and the per-segment adaptive energy detector: the cascade is suited for sustained continuous transmissions, while the adaptive variant recovers discriminability under intermittent low-duty-cycle protocols, suggesting their combined use as complementary front-ends in heterogeneous deployment scenarios.

The study identifies four explicit limitations: reliance on a single controlled dataset, post-chunking application of stress tests, inapplicability to low-duty-cycle transmission protocols, and absence of real-time streaming evaluation. Future work will address these through evaluation on more diverse RF datasets, adaptive burst length thresholding for intermittent signals, and real-time implementation on resource-constrained hardware.

Overall, the proposed method connects classical signal processing techniques with the practical requirements of UAV RF monitoring. By combining burst-aware temporal reasoning with selective high-cost analysis, it provides a transparent and scalable detection approach that is well-suited for continuous spectrum monitoring and can serve as a front-end module within larger UAV identification or RF situational awareness systems.

Author Contributions: Conceptualization, I.S., O.K., Y.K. and I.A.; Methodology, I.S., O.K., Y.K. and I.A.; Software, O.K., I.A. and A.A.; Validation, O.K. and I.A.; Formal analysis, O.K., Y.K. and I.A.; Investigation, I.S. and Y.K.; Data curation, A.A.; Writing—original draft, O.K. and A.A.; Writing—review & editing, A.A. All authors have read and agreed to the published version of the manuscript.

Funding: This research received no external funding.

Institutional Review Board Statement: Not applicable.

Informed Consent Statement: Not applicable.

Data Availability Statement: The source code and supporting scripts used to perform data preprocessing, method implementation, evaluation, and figure generation for this work are publicly available in a dedicated GitHub repository. This repository provides full reproducibility of the experimental results reported in the manuscript and includes notebooks, utility modules, and configuration files corresponding to each stage of the pipeline. Access the repository at: https://github.com/owlvano/rfml-uav/tree/main/notebooks/paper2-cascade-detection-method (accessed on 28 May 2026). The code is released under the GNU General Public License v3.0 (GPL-3.0), which permits use, modification, and redistribution for research and non-commercial purposes, provided that derivative works are distributed under the same license and proper attribution is given. The repository is documented with README files at the root and within subdirectories, detailing the code structure, dependency installation instructions, and step-by-step usage guidelines. Inline comments and docstrings are provided to clarify algorithmic steps and parameter choices. The code is released under a permissive li-cense to facilitate reuse and extension by the research community.

Acknowledgments: Generative artificial intelligence tools were used to assist with language refinement and structural organization of the manuscript. These tools were employed solely to improve clarity, coherence, and presentation of the text. No generative AI tools were used for data generation, algorithm design, experimental execution, or interpretation of the experimental results. All methodological decisions, data processing, analysis, and conclusions presented in this work were developed and validated by the authors.

Conflicts of Interest: The authors declare no conflict of interest.

Abbreviations

The following abbreviations are used in this manuscript:

UAV	Unmanned aerial vehicle
RF	Radio frequency
SCF	Spectral correlation function
AUC	Area under the ROC curve
P_d	Probability of detection
P_{fa}	Probability of false alarm
ISM	Industrial, scientific and medical (radio band)
BUI	Binary unique identifier
DWT	Discrete wavelet transform
STFT	Short-time Fourier transform
DFT	Discrete Fourier transform
FFT	Fast Fourier transform
SNR	Signal-to-noise ratio
MAD	Median absolute deviation
CNN	Convolutional neural network
ReLU	Rectified linear unit
PSD	Power spectral density
AED	Adaptive energy detector
ROC	Receiver operating characteristic
DSSS	Direct-sequence spread spectrum
OFDM	Orthogonal frequency-division multiplexing

References

1. Wang, Y.; Chen, M.; Pan, C.; Wang, K.; Pan, Y. Joint Optimization of UAV Trajectory and Sensor Uploading Powers for UAV-Assisted Data Collection in Wireless Sensor Networks. *IEEE Int. Things J.* **2022**, *9*, 11214–11226. [CrossRef]
2. Skakodub, O.; Kozlov, O.; Kondratenko, Y. Optimization of Linguistic Terms' Shapes and Parameters: Fuzzy Control System of a Quadrotor Drone. In *Proceedings of the 2021 11th IEEE International Conference on Intelligent Data Acquisition and Advanced Computing Systems: Technology and Applications (IDAACS)*; IEEE: New York, NY, USA, 2021; Volume 1, pp. 566–571.
3. Kozlov, O.; Kondratenko, G.; Aleksieieva, A.; Maksymov, M.; Tarakhtij, O. *Swarm Optimization of the Drone's Intelligent Control System: Comparative Analysis of Hybrid Techniques*; CEUR Workshop Proceedings: Bonn, Germany, 2024; Volume 3790, pp. 1–12.
4. Lykou, G.; Moustakas, D.; Gritzalis, D. Defending Airports from UAS: A Survey on Cyber-Attacks and Counter-Drone Sensing Technologies. *Sensors* **2020**, *20*, 3537. [CrossRef]
5. Hadi, H.J.; Cao, Y.; Nisa, K.U.; Jamil, A.M.; Ni, Q. A Comprehensive Survey on Security, Privacy Issues and Emerging Defence Technologies for UAVs. *J. Netw. Comput. Appl.* **2023**, *213*, 103607. [CrossRef]
6. Cordill, B.; Fang, D.; Xu, S. A Comprehensive Survey of Security and Privacy in UAV Systems. *IEEE Access* **2025**, *13*, 117843–117866. [CrossRef]
7. Tang, Z.; Ma, H.; Qu, Y.; Mao, X. UAV Detection with Passive Radar: Algorithms, Applications, and Challenges. *Drones* **2025**, *9*, 76. [CrossRef]
8. Yan, X.; Fu, T.; Lin, H.; Xuan, F.; Huang, Y.; Cao, Y.; Hu, H.; Liu, P. UAV Detection and Tracking in Urban Environments Using Passive Sensors: A Survey. *Appl. Sci.* **2023**, *13*, 11320. [CrossRef]
9. Han, M.; Yang, H.; Li, W.; Xu, W.; Cheng, X.; Mohapatra, P.; Hu, P. RF Sensing Security and Malicious Exploitation: A Comprehensive Survey. *arXiv* **2025**, arXiv:2504.10969. [CrossRef]
10. Casmin, E.; Oliveira, R. Survey on Context-Aware Radio Frequency-Based Sensing. *Sensors* **2025**, *25*, 602. [CrossRef] [PubMed]
11. Khawaja, W.; Ezuma, M.; Semkin, V.; Erden, F.; Ozdemir, O.; Guvenc, I. A Survey on Detection, Classification, and Tracking of AAVs Using Radar and Communications Systems. *IEEE Commun. Surv. Tutor.* **2026**, *28*, 3272–3310. [CrossRef]
12. Ezuma, M.; Erden, F.; Anjinappa, C.K.; Ozdemir, O.; Guvenc, I. Micro-UAV Detection and Classification from RF Fingerprints Using Machine Learning Techniques. In *Proceedings of the 2019 IEEE Aerospace Conference*; IEEE: New York, NY, USA, 2019; pp. 1–13.
13. Al-Hourani, A.; Kandeepan, S.; Jamalipour, A. Modeling Air-to-Ground Path Loss for Low Altitude Platforms in Urban Environments. In *Proceedings of the 2014 IEEE Global Communications Conference*; IEEE: New York, NY, USA, 2014; pp. 2898–2904.

14. Sahai, A.; Hoven, N.K.; Tandra, R. Some Fundamental Limits on Cognitive Radio. In Proceedings of the 42nd Allerton Conference on Communication, Control, and Computing, Monticello, IL, USA, 29 September–1 October 2004.
15. Tandra, R.; Sahai, A. Fundamental Limits on Detection in Low SNR under Noise Uncertainty. In *Proceedings of the 2005 International Conference on Wireless Networks, Communications and Mobile Computing*; IEEE: New York, NY, USA, 2005; Volume 1, pp. 464–469.
16. Valadão, M.; Amoedo, D.; Costa, A.; Carvalho, C.; Sabino, W. Predicting Noise and User Distances from Spectrum Sensing Signals Using Transformer and Regression Models. *Appl. Sci.* **2025**, *15*, 4296. [CrossRef]
17. Alam, S.S.; Chakma, A.; Rahman, M.H.; Bin Mofidul, R.; Alam, M.M.; Utama, I.B.; Jang, Y.M. RF-Enabled Deep-Learning-Assisted Drone Detection and Identification: An End-to-End Approach. *Sensors* **2023**, *23*, 4202. [CrossRef]
18. Al-Sa'd, M.F.; Al-Ali, A.; Mohamed, A.; Khattab, T.; Erbad, A. RF-Based Drone Detection and Identification Using Deep Learning Approaches: An Initiative towards a Large Open Source Drone Database. *Future Gener. Comput. Syst.* **2019**, *100*, 86–97. [CrossRef]
19. Ni, T.; Ding, X.; Wang, Y.; Shen, J.; Jiang, L.; Zhang, G. Spectrum Sensing via Temporal Convolutional Network. *China Commun.* **2021**, *18*, 37–47. [CrossRef]
20. Axell, E.; Leus, G.; Larsson, E.G.; Vincent Poor, H. Spectrum Sensing for Cognitive Radio: State-of-the-Art and Recent Advances. *IEEE Signal Process. Mag.* **2012**, *29*, 101–116. [CrossRef]
21. Yucek, T.; Arslan, H. A Survey of Spectrum Sensing Algorithms for Cognitive Radio Applications. *IEEE Commun. Surv. Tutor.* **2009**, *11*, 116–130. [CrossRef]
22. Urkowitz, H. Energy Detection of Unknown Deterministic Signals. *Proc. IEEE* **1967**, *55*, 523–531. [CrossRef]
23. Salt, J.E.; Nguyen, H.H. Performance Prediction for Energy Detection of Unknown Signals. *IEEE Trans. Veh. Technol.* **2008**, *57*, 3900–3904. [CrossRef]
24. Oh, H.; Nam, H. Energy Detection Scheme in the Presence of Burst Signals. *IEEE Signal Process. Lett.* **2019**, *26*, 582–586. [CrossRef]
25. Huang, H.; Zhu, J.; Mu, J. A Novel Sensing Strategy Based on Energy Detector for Spectrum Sensing. *Appl. Sci.* **2019**, *9*, 4634. [CrossRef]
26. Al-Dulaimi, O.M.K.; Chiper, F.-L.; Vlădeanu, C.; Martian, A. Triple- Threshold Energy Detection with Adaptive Intermediate Threshold for Cooperative Spectrum Sensing. In *Proceedings of the 2022 14th International Conference on Communications (COMM)*; IEEE: New York, NY, USA, 2022; pp. 1–6.
27. Nikonowicz, J.; Kubczak, P.; Matuszewski, Ł. Hybrid Detection Based on Energy and Entropy Analysis as a Novel Approach for Spectrum Sensing. In *Proceedings of the 2016 International Conference on Signals and Electronic Systems (ICSES)*; IEEE: New York, NY, USA, 2016; pp. 206–211.
28. Wang, W.; Wang, J.; Li, C. A Signal Detection Method Based on Hybrid Energy Detection. In *Proceedings of the 2022 4th International Conference on Intelligent Control, Measurement and Signal Processing (ICMSP)*; IEEE: New York, NY, USA, 2022; pp. 695–700.
29. Qiao, G.; Bilal, M.; Liu, S.; Babar, Z.; Ma, T. Biologically Inspired Covert Underwater Acoustic Communication—A Review. *Phys. Commun.* **2018**, *30*, 107–114. [CrossRef]
30. Liu, S.; Zuberi, H.H.; Arfeen, Z.; Zhang, X.; Bilal, M.; Sun, Z. Spectral Efficient Neural Network-Based M-Ary Chirp Spread Spectrum Receivers for Underwater Acoustic Communication. *Arab. J. Sci. Eng.* **2024**, *49*, 16593–16609. [CrossRef]
31. Gardner, W.A.; Napolitano, A.; Paura, L. Cyclostationarity: Half a Century of Research. *Signal Process.* **2006**, *86*, 639–697. [CrossRef]
32. Napolitano, A. Cyclostationary Processes and Time Series. In *Theory, Applications, and Generalizations*; Academic Press: London, UK, 2019; ISBN 978-0-08-102708-0.
33. Cheng, H.; Mark, B.L.; Ephraim, Y. Wideband Temporal Spectrum Sensing Using Cepstral Features. In *Proceedings of the 2019 IEEE 20th International Symposium on "A World of Wireless, Mobile and Multimedia Networks" (WoWMoM)*; IEEE: New York, NY, USA, 2019; pp. 1–6.
34. Yang, Y.; Ji, Y.L.; Li, H.H.; Lei, D.; Rui, M. Adaptive Two-Stage Sensing Based on Energy Detection and Cyclostationary Feature Detection for Cognitive Radio Systems. *Appl. Mech. Mater.* **2013**, *411–414*, 1521–1528. [CrossRef]
35. Bagwari, A.; Tomar, G.S. Two-Stage Detectors with Multiple Energy Detectors and Adaptive Double Threshold in Cognitive Radio Networks. *Int. J. Distrib. Sens. Netw.* **2013**, *9*, 656495. [CrossRef]
36. Mourougayane, K.; Amgothu, B.; Bhagat, S.; Srikanth, S. A Robust Multistage Spectrum Sensing Model for Cognitive Radio Applications. *AEU-Int. J. Electron. Commun.* **2019**, *110*, 152876. [CrossRef]
37. Sejdić, E.; Djurović, I.; Jiang, J. Time–Frequency Feature Representation Using Energy Concentration: An Overview of Recent Advances. *Digit. Signal Process.* **2009**, *19*, 153–183. [CrossRef]
38. Brewster, M.E. An Introduction to Wavelets (Charles K. Chui). *SIAM Rev.* **1993**, *35*, 312–313. [CrossRef] [PubMed]
39. Muchandi, N.; Khanai, R. Cognitive Radio Spectrum Sensing: A Survey. In *Proceedings of the 2016 International Conference on Electrical, Electronics, and Optimization Techniques (ICEEOT)*; IEEE: New York, NY, USA, 2016; pp. 3233–3237.
40. Sani, M.; Tsado, J.; Thomas, S.; Suleiman, H.; Shehu, I.M.; Shan'una, M.G. A Survey on Spectrum Sensing Techniques for Cognitive Radio Networks. In *Proceedings of the 2021 1st International Conference on Multidisciplinary Engineering and Applied Science (ICMEAS)*; IEEE: New York, NY, USA, 2021; pp. 1–5.

41. Abbate, A.; Koay, J.; Frankel, J.; Schroeder, S.C.; Das, P. Signal Detection and Noise Suppression Using a Wavelet Transform Signal Processor: Application to Ultrasonic Flaw Detection. *IEEE Trans. Ultrason. Ferroelectr. Freq. Control* **1997**, *44*, 14–26. [CrossRef] [PubMed]
42. Zhang, X.; Hu, C. Research of Singular Signal Detection Based on Wavelet Analysis. In *Proceedings of the 2010 6th International Conference on Wireless Communications Networking and Mobile Computing (WiCOM)*; IEEE: New York, NY, USA, 2010; pp. 1–4.
43. Lysechko, V.; Soproniuk, I. Spectrum Sensing Using Wavelet Transforms and Filtering Under Signal Frequency Distortion and Fading Conditions. *SISIOT* **2024**, *2*, 01011. [CrossRef]
44. Akansu, A.N.; Haddad, R.A. Chapter 6—Wavelet Transform. In *Multiresolution Signal Decomposition (Second Edition)*; Academic Press: San Diego, CA, USA, 2001; pp. 391–442, ISBN 978-0-12-047141-6.
45. O'Shea, T.J.; Corgan, J.; Clancy, T.C. Convolutional Radio Modulation Recognition Networks. In *Proceedings of the Engineering Applications of Neural Networks*; Jayne, C., Iliadis, L., Eds.; Springer International Publishing: Cham, Switzerland, 2016; pp. 213–226.
46. Al-Emadi, S.; Al-Senaid, F. Drone Detection Approach Based on Radio-Frequency Using Convolutional Neural Network. In *Proceedings of the 2020 IEEE International Conference on Informatics, IoT, and Enabling Technologies (ICIoT)*; IEEE: New York, NY, USA, 2020; pp. 29–34.
47. Archana, P.; Karthigaikumar, P. Machine Learning and Transfer Learning Based Spectrum Sensing in Cognitive Radio Networks. In *Proceedings of the 2024 IEEE 11th Uttar Pradesh Section International Conference on Electrical, Electronics and Computer Engineering (UPCON)*; IEEE: New York, NY, USA, 2024; pp. 1–5.
48. Zhao, C.; Chen, C.; He, Z.; Wu, Z. Application of Auxiliary Classifier Wasserstein Generative Adversarial Networks in Wireless Signal Classification of Illegal Unmanned Aerial Vehicles. *Appl. Sci.* **2018**, *8*, 2664. [CrossRef]
49. Ul Qamar, M.S.; Akhter, M.A.; Nawaz, R. Automatic Modulation Recognition Using Convolutional Neural Networks. In *Proceedings of the 2022 19th International Bhurban Conference on Applied Sciences and Technology (IBCAST)*; IEEE: New York, NY, USA, 2022; pp. 490–493.
50. Kondratenko, Y.; Sova, I.; Kozlov, O.; Kuzmenko, V. *Identification of Unmanned Aerial Vehicles Using RF Fingerprinting and Deep Learning Networks*; CEUR Workshop Proceedings: Bonn, Germany, 2025; Volume 4004, pp. 312–326.
51. Roy, D.; Mukherjee, T.; Chatterjee, M.; Pasiliao, E. Detection of Rogue RF Transmitters Using Generative Adversarial Nets. In *Proceedings of the 2019 IEEE Wireless Communications and Networking Conference (WCNC)*; IEEE: New York, NY, USA, 2019; pp. 1–7.
52. Xun, D.T.W.; Lim, Y.L.; Srigrarom, S. Drone Detection Using YOLOv3 with Transfer Learning on NVIDIA Jetson TX2. In *Proceedings of the 2021 Second International Symposium on Instrumentation, Control, Artificial Intelligence, and Robotics (ICA-SYMP)*; IEEE: New York, NY, USA, 2021; pp. 1–6.
53. Gang, Q.; Rahman, W.U.; Zhou, F.; Bilal, M.; Ali, W.; Khan, S.U.; Khattak, M.I. A Q-Learning-Based Approach to Design an Energy-Efficient MAC Protocol for UWSNs Through Collision Avoidance. *Electronics* **2024**, *13*, 4388. [CrossRef]
54. Fawzi, A.; El-Shafai, W.; Abd-Elnaby, M.; Zekry, A.; Abd El-Samie, F.E. Adaptive Two-Stage Spectrum Sensing Model Using Energy Detection and Wavelet Denoising for Cognitive Radio Systems. *Int. J. Commun. Syst.* **2020**, *33*, e4400. [CrossRef]
55. Ezuma, M.; Erden, F.; Kumar Anjinappa, C.; Ozdemir, O.; Guvenc, I. Detection and Classification of UAVs Using RF Fingerprints in the Presence of Wi-Fi and Bluetooth Interference. *IEEE Open J. Commun. Soc.* **2020**, *1*, 60–76. [CrossRef]
56. Mo, Y.; Huang, J.; Qian, G. Deep Learning Approach to UAV Detection and Classification by Using Compressively Sensed RF Signal. *Sensors* **2022**, *22*, 3072. [CrossRef]
57. López-Benítez, M.; Casadevall, F. Time-Dimension Models of Spectrum Usage for the Analysis, Design, and Simulation of Cognitive Radio Networks. *IEEE Trans. Veh. Technol.* **2013**, *62*, 2091–2104. [CrossRef]

Disclaimer/Publisher's Note: The statements, opinions and data contained in all publications are solely those of the individual author(s) and contributor(s) and not of MDPI and/or the editor(s). MDPI and/or the editor(s) disclaim responsibility for any injury to people or property resulting from any ideas, methods, instructions or products referred to in the content.